Chapter 7

Large-eddy simulations: theory and applications

by
Ugo Piomelli
University of Maryland
College Park, Maryland, USA

and
Jeffrey R. Chasnov
The Hong Kong University of Science & Technology
Clear Water Bay, Kowloon, HONG KONG

7.1 Introduction

Over twenty years have passed since the first large eddy simulation (LES) results by Deardorff (1970) were published. During this period, this technique has matured considerably: the underlying theory has been advanced, new models have been developed and tested, more efficient numerical schemes have been used. The progress in computer power and memory has made possible the application of LES to a variety of flows, compressible and incompressible, including heat transfer, stratification, passive scalars and chemical reactions.

Turbulence is a phenomenon that occurs frequently in nature; it has, therefore, been the subject of study for over one hundred years. In present days, the prediction and control of turbulent flows has become increasingly important, due to their frequent occurrence in technological applications involving transportation systems (cars, aircraft and ships), energy conversion systems (engines, turbines, compressors) and geophysical applications (weather prediction, pollutant dispersion). The need for accurate models of turbulent flows is presently the pacing item for the development of more accurate design and analysis tools for the applications

mentioned above. For these reasons, added stress has been placed in recent years on the development of accurate numerical tools for the prediction of turbulent flows.

Analytical or numerical solution of turbulent flow problems can be accomplished using various levels of approximation, yielding more or less detailed descriptions of the state of the flow. The simplest approach is to use semi-empirical correlations. Moody's diagram, which gives the skin friction factor for cylindrical pipes as a function of Reynolds number and relative roughness, is an example of this approach, which is especially useful for global, control-volume analyses, but that yields no information on local quantities and relies heavily on the availability of experimental data in configurations similar to the one under study.

A more sophisticated method involves the application of Reynolds' averaging to the equations of motion to obtain the well-known Reynolds-averaged Navier-Stokes equations, that describe the evolution of the mean quantities. The effect of turbulent fluctuations appears in a Reynolds stress term $\langle u_i' u_j' \rangle$ that must be modeled to close the system. The most commonly used models for the Reynolds-averaged Navier-Stokes (RANS) equations, however, lack generality: the model constants are usually set using a few simple flows, for which theoretical solutions are known or well-documented experiments are available. When the models are applied to flows that are very different from the ones used for calibration, however, the constants often have to be adjusted to yield accurate predictions. Furthermore, laminar-turbulent transition is exceedingly difficult to predict using the RANS approach, and requires the addition of significant semi-empirical data, usually in the form of intermittency functions. The principal reason for the lack of generality of turbulence models lies in the fact that the model must represent a very wide range of scales. While the small scales tend to depend only on viscosity, and may be somewhat universal, the large ones are affected very strongly by the boundary conditions (see, for instance, the difference between the spanwise rollers present in mixing layers and wakes and the elongated streamwise vortices that are found in the near-wall region of a turbulent boundary layer). Thus, it does not seem possible to model the effect of the large scales of turbulence in the same way in flows that are very different.

The most straightforward approach to the solution of turbulent flows is the direct numerical simulation (DNS) of turbulence, in which the governing equations are discretized and solved numerically. If the mesh is fine enough to resolve even the smallest scales of motion, and the scheme is designed to minimize the numerical dispersion and dissipation errors, one can obtain an accurate three-dimensional, time-dependent solution of the governing equations completely free of modeling assumptions, and in which the only errors are those introduced by the numerical approximation. DNS has been a very useful tool, over the past ten years, for the study of transitional and turbulent flow physics, but it also has some serious limitations. First, the use of highly accurate, high-order schemes is desirable to limit dispersion and dissipation errors; these schemes (spectral methods, for example) tend to have little flexibility in handling complex geometries and general boundary conditions. Secondly, to resolve all scales of motion, one requires a

number of grid points $N \sim L/\eta$, where L is the dimension of the computational domain (the largest scale in the system) and η is the smallest scale of motion, the Kolmogorov length scale. Since this ratio is proportional to $Re^{3/4}$, the number of grid points required by a DNS goes like $N^3 \sim Re^{9/4}$; furthermore, the number of timesteps required to advance the computation for a given period scales like $Re^{3/4}$. Assuming that the cost of a computation per time step scales at least with the number of grid points, then the total cost of a direct simulation is proportional to Re^3. Thus, to increase the Reynolds number by a factor of two, the computational effort must increase by at least a factor of 8. For these reasons, DNS has largely been limited to simple geometries (flat plate, homogeneous flows) at low Reynolds numbers, and its application to engineering-type problems within the next decade appears unlikely.

Large-eddy simulation (LES) is a technique intermediate between the direct simulation of turbulent flows and the solution of the Reynolds-averaged equations. In LES the contribution of the large, energy-carrying structures to momentum and energy transfer is computed exactly, and only the effect of the smallest scales of turbulence is modeled. Since the small scales tend to be more homogeneous and universal, and less affected by the boundary conditions than the large ones, there is hope that their models can be simpler and require fewer adjustments when applied to different flows than similar models for the RANS equations. LES is similar to DNS in that it provides a three-dimensional, time dependent solution of the Navier-Stokes equations. Thus, it still requires fairly fine meshes. However, it can be used at much higher Reynolds numbers than DNS; ideally, in fact, if the small scales obey inertial range dynamics, the cost of a computation is independent of Re (not, however, if a solid boundary is present). In the following sections various aspects of the theory of LES will be discussed and some applications will be presented.

7.2 Governing equations and filters

7.2.1 The filtering operation

LES is based on the definition of a filtering operation: a filtered (or resolved, or large-scale) variable, denoted by an overbar, is defined as

$$\overline{f}(\vec{x}) = \int_D f(\vec{x}')G(\vec{x},\vec{x}')d\vec{x}', \tag{7.1}$$

where D is the entire domain and G is the *filter* function. The filter function determines the size and structure of the small scales. It is easy to show that, if G is a function of $x - x'$ only, differentiation and the filtering operation commute (Leonard 1974).

The most commonly-used filter functions are the sharp Fourier cutoff filter,

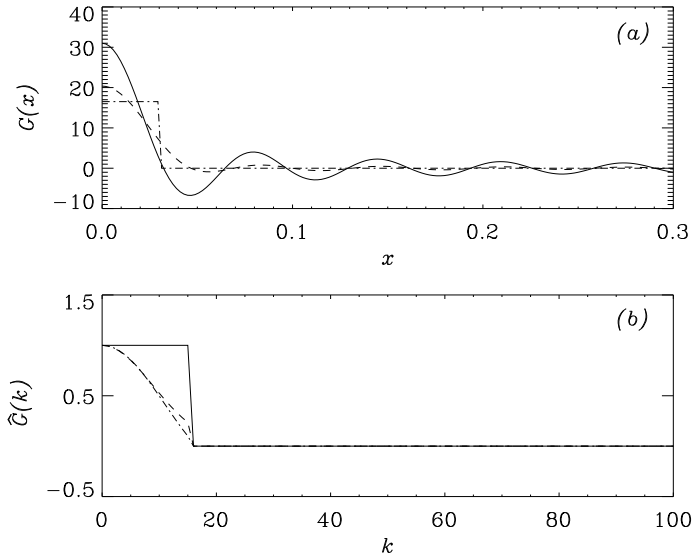

Figure 7.1: Typical filter functions. ——— : sharp Fourier cutoff; - - - : truncated Gaussian; —·— : tophat. (a) real space; (b) Fourier space.

best defined in wave space[1] as

$$\widehat{G}(k) = \begin{cases} 1 & \text{if } k \leq \pi/\Delta \\ 0 & \text{otherwise,} \end{cases} \tag{7.2}$$

the Gaussian filter,

$$G(x) = \sqrt{\frac{6}{\pi\Delta^2}} \exp\left(-\frac{6x^2}{\Delta^2}\right), \tag{7.3}$$

and the tophat filter in real space:

$$G(x) = \begin{cases} 1/\Delta & \text{if } |x| \leq \Delta/2 \\ 0 & \text{otherwise,} \end{cases} \tag{7.4}$$

these three filters and their Fourier transforms are shown in Figure 7.1. It should be noticed that the Gaussian filter is used in conjunction with a sharp Fourier cutoff. The truncation of the Gaussian at a non-negligible value is the cause for the ringing observed in the figure. For uniform filter width[2] Δ the filters above are mean-preserving and commute with differentiation.

To illustrate the difference between the filters defined above they are applied to a test function; the spectra of the filtered variables are shown in Figure 7.2. The Tophat and Gaussian filters give similar results; in particular, they both smooth the large-scale fluctuations as well as the small-scale ones, unlike the Fourier cutoff, that only affects the scales below the cutoff wavenumber.

[1] Unless otherwise noted, a quantity denoted by a caret $\widehat{\cdot}$ is the complex Fourier coefficient of the original quantity.

[2] For a discussion of filtering with non-uniform filters see Ghosal and Moin (1995).

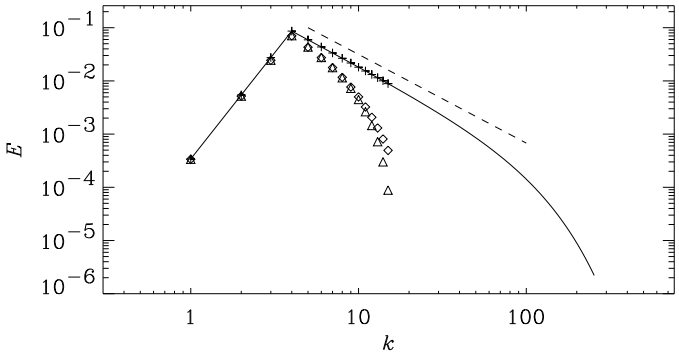

Figure 7.2: Filtering of a test function. ——— : Unfiltered; --- $k^{-5/3}$; + : sharp Fourier cutoff; ◇ : Gaussian; △ : tophat.

7.2.2 Filtered Navier-Stokes equations

If the filtering operation (7.1) is applied to the governing equations, one obtains the filtered equations of motion. For an incompressible flow of a Newtonian fluid, they take the following form:

$$\frac{\partial \overline{u}_i}{\partial x_i} = 0. \tag{7.5}$$

$$\frac{\partial \overline{u}_i}{\partial t} + \frac{\partial}{\partial x_j}\left(\overline{u}_i \overline{u}_j\right) = -\frac{1}{\rho}\frac{\partial \overline{p}}{\partial x_i} - \frac{\partial \tau_{ij}}{\partial x_j} + \nu \frac{\partial^2 \overline{u}_i}{\partial x_j \partial x_j}. \tag{7.6}$$

$$\tag{7.7}$$

The filtered Navier-Stokes equations govern the evolution of the large, energy-carrying, scales of motion. The effect of the small scales appears through a subgrid-scale (SGS) stress term,

$$\tau_{ij} = \overline{u_i u_j} - \overline{u}_i \overline{u}_j, \tag{7.8}$$

that must be modeled.

If the subgrid scale velocity $u_i' = u_i - \overline{u}_i$ is defined, the SGS stresses can be decomposed into three parts (Leonard 1974):

$$\tau_{ij} = \overline{u_i u_j} - \overline{u}_i \overline{u}_j = L_{ij} + C_{ij} + R_{ij}, \tag{7.9}$$

where $L_{ij} = \overline{\overline{u}_i \overline{u}_j} - \overline{u}_i \overline{u}_j$ are the Leonard stresses, $C_{ij} = \overline{\overline{u}_i u_j'} + \overline{u_j' \overline{u}_i}$ are the cross terms, and $R_{ij} = \overline{u_i' u_j'}$ are the SGS Reynolds stresses. The Leonard stresses represent interactions between resolved scales that result in subgrid-scale contributions. They can be computed explicitly, and, when the sharp cutoff filter is used they are the aliasing errors. The cross terms represent interactions between resolved and unresolved scales, whereas the SGS Reynolds stresses represent interactions between small, unresolved, scales. While the SGS stresses τ_{ij} are invariant with respect to a Galilean transformation, neither L_{ij} nor C_{ij} are (Speziale 1985). For

this and other reasons (see Germano 1986), the decomposition (7.9) has largely been abandoned.

For later use the Fourier transform of the filtered Navier-Stokes equations will be introduced. Assuming turbulence in a periodic box of length 2π, the velocity field may be transformed as

$$u_i(\vec{x},t) = \sum_{\vec{k}} \widehat{u}_i(\vec{k},t) \exp\left(i\vec{k}\cdot\vec{x}\right), \tag{7.10}$$

where $\widehat{u}_i(\vec{k})$ is the Fourier transform of $u_i(\vec{x})$, $\vec{k} = (n_1, n_2, n_3)$, and the summation is over all integer values of n_1, n_2, and n_3. Using the sharp Fourier cutoff filter (7.2) and defining $k_m = \pi/\Delta$, one obtains the Fourier transform of the filtered Navier-Stokes equations, applicable for wavenumbers $k \leq k_m$:

$$\begin{aligned} \frac{\partial \widehat{u}_i(\vec{k},t)}{\partial t} \quad &+ \quad \nu k^2 \widehat{u}_i(\vec{k},t) = \\ &- \quad ik_n P_{ij}(\vec{k}) \left[\sum_{\substack{\vec{p}+\vec{q}=\vec{k} \\ p,q \leq k_m}} \widehat{u}_n(\vec{p})\widehat{u}_j(\vec{q}) + \sum_{\substack{\vec{p}+\vec{q}=\vec{k} \\ p \text{ or } q > k_m}} \widehat{u}_n(\vec{p})\widehat{u}_j(\vec{q}) \right]. \end{aligned} \tag{7.11}$$

The pressure has been eliminated from (7.11) using the Fourier transform of (7.5). The influence of the subgrid scales appears in the last summation of (7.11) . This summmation includes contributions from both the cross-term (only one of $\vec{p}$ or $\vec{q}$ greater than k_m) and the SGS Reynolds stresses (both $\vec{p}$ and $\vec{q}$ greater than k_m). The Leonard stresses vanish identically when using the Fourier cutoff filter.

7.2.3 Energy equations

It is useful, in order to develop SGS models, to understand the physical phenomena that the models should represent. Arguably, the most important effect of the subgrid scales on the large ones, and the one that the model must represent accurately, is the energy exchange that results from the interaction between resolved and unresolved scales. To understand this interaction better, consider the transport equations for $\overline{q}^2 = \overline{u}_i\overline{u}_i$, twice the total resolved energy (mean and fluctuating), and $q_{sgs}^2 = \tau_{kk}$, twice the subgrid-scale kinetic energy:

$$\begin{aligned} \frac{\partial \overline{q}^2}{\partial t} \quad &+ \quad \underbrace{\frac{\partial}{\partial x_j}(\overline{q}^2\overline{u}_j)}_{\text{Advection of } \overline{q}^2} = -2 \quad \underbrace{\frac{\partial}{\partial x_j}(\overline{p}\,\overline{u}_j)}_{\text{Press. Diff. of } \overline{q}^2} + \underbrace{\frac{\partial}{\partial x_j}\left(\nu \frac{\partial \overline{q}^2}{\partial x_j}\right)}_{\text{Visc. Diff. of } \overline{q}^2} \\ &-2 \underbrace{\frac{\partial}{\partial x_j}(\tau_{ij}\overline{u}_i)}_{\text{SGS Diff.}} - 2 \quad \underbrace{\nu \frac{\partial \overline{u}_i}{\partial x_j}\frac{\partial \overline{u}_i}{\partial x_j}}_{\text{Visc. Diss. of } \overline{q}^2} + 2 \quad \underbrace{\tau_{ij}\overline{S}_{ij}}_{\text{SGS Diss.}} \end{aligned} \tag{7.12}$$

$$\frac{\partial q^2_{sgs}}{\partial t} + \underbrace{\frac{\partial}{\partial x_j}(q^2_{sgs}\overline{u}_j)}_{\text{Advection of } q^2_{sgs}} = \underbrace{-\frac{\partial}{\partial x_j}(\overline{u_i u_i u_j} - \overline{u_i u_i}\,\overline{u}_j)}_{\text{Turb. Transport}} \underbrace{-2\,\frac{\partial}{\partial x_j}(\overline{p u_j} - \overline{p}\,\overline{u}_j)}_{\text{Press. Diff. of } q^2_{sgs}}$$
$$+ \underbrace{\frac{\partial}{\partial x_j}\left(\nu \frac{\partial q^2_{sgs}}{\partial x_j}\right)}_{\text{Visc. Diff. of } q^2_{sgs}} \underbrace{+2\,\frac{\partial}{\partial x_j}(\tau_{ij}\overline{u}_i)}_{\text{SGS Diff.}}$$
$$\underbrace{-2\,\nu\left(\overline{\frac{\partial u_i}{\partial x_j}\frac{\partial u_i}{\partial x_j}} - \frac{\partial \overline{u}_i}{\partial x_j}\frac{\partial \overline{u}_i}{\partial x_j}\right)}_{\text{Visc. Diss. of } q^2_{sgs}} \underbrace{-2\;\tau_{ij}\overline{S}_{ij}}_{\text{SGS Diss.}} . \tag{7.13}$$

The equations above show that the resolved scales in a control volume (a grid cell, for example), exchange energy with the unresolved scales and the surroundings through several mechanisms. The advection and diffusion terms do not create or destroy resolved energy but only redistribute it between adjoining volumes. The last two terms in (7.12) represent respectively the resolved energy lost by viscous dissipation at the resolved-scale level, and the net energy exchange between the resolved and unresolved scales. Although the subgrid-scale dissipation $\varepsilon_{sgs} = \tau_{ij}\overline{S}_{ij}$ can be positive or negative, on the average energy flows from the large to the small scales, and $\varepsilon_{sgs} < 0$ (forward scatter); backscatter occurs when the energy flow is reversed ($\varepsilon_{sgs} > 0$). The total transfer of energy between large and subgrid scales is the SGS transfer, sum of SGS diffusion and dissipation.

The energy exchange mechanisms for the subgrid scales are similar; the advection and diffusion ters are again redistribution terms. The energy lost by the resolved scales to the subgrid ones appears as a source term in the transport equation for q^2_{sgs}: the SGS diffusion and dissipation have opposite signs in (7.12) and (7.13). It is important to point out the difference between the viscous and SGS dissipation of SGS energy. The SGS dissipation ε_{sgs} represents an energy interchange between resolved and unresolved scales, and is generally a dissipative term in the equation for $\overline{q}^2$, a production term in the equation for q^2_{sgs}. The viscous dissipation, ε_v, on the other hand, represents the SGS energy dissipated by the viscous forces.

A spectral energy equation may also be developed from (7.11). Multiplying (7.11) by the complex conjugate of $\widehat{u}(\vec{k},t)$, and adding the resulting equation to the complex conjugate of (7.11) multiplied by $\widehat{u}(\vec{k},t)$, one obtains, after integrating over the angles of $\vec{k}$,

$$\frac{\partial E(k,t)}{\partial t} + 2\nu k^2 E(k) = T_{\rm res}(k,t) + T_{\rm sub}(k,t)\,. \tag{7.14}$$

The resolved scale transfer spectrum $T_{\rm res}(k,t)$ arises from the first summation in (7.11) and the subgrid scale transfer spectrum $T_{\rm sub}(k,t)$ from the second summation. $T_{\rm res}(k,t)$ is responsible for the nonlinear transfer of energy among wavenumbers with magnitude less than k_m, whereas $T_{\rm sub}(k,t)$ transfers energy between

wavenumbers with magnitude less than k_m and those greater than k_m. A negative value of $T_{\rm sub}(k,t)$ signifies a transfer of energy from the resolved scales to the subgrid scales, and positive values signify a backscatter of energy from subgrid scales to resolved scales.

7.3 Principles of small scale modeling

7.3.1 Universality of small scales

Kolmogorov's theory of the inertial subrange stands as one of the most important and influential results in turbulence physics. The essence of the Kolmogorov theory is quite simple: turbulence generation occurs mainly at the largest scales of a flow and viscous dissipation occurs mainly at the smallest scales, leaving a range of scale sizes at high Reynolds numbers — the so-called inertial subrange — over which external influences (frictional boundaries, body forces, initial conditions) and viscosity are negligible. These scale sizes obtain turbulent kinetic energy only by nonlinear transfer of energy from larger scale sizes, and lose energy by subsequent transfer to smaller scale sizes. The only dimensional quantity of importance for these intermediate wave numbers is the flux of energy from large-to-small scale sizes, or equivalently, from small-to-large wavenumbers. Since all energy is eventually dissipated in the flow by molecular viscosity, this flux of energy must be equal to the rate of energy dissipation, commonly denoted by ε. Dimensionally, $[\varepsilon] = l^2/t^3$, where l is a length and t is a time, and since the three-dimensional energy spectrum $E(k)$ has dimensions $[E] = l^3/t^2$, one determines

$$E(k) = \mathrm{Ko}\,\varepsilon^{\frac{2}{3}} k^{-\frac{5}{3}} \,, \tag{7.15}$$

where Ko is the Kolmogorov constant. The published values of Ko, determined by experiment and numerical simulation, lie mainly between 1.4 and 2.1, the scatter being primarily due to the difficulty in measuring ε, and of obtaining sufficiently high Reynolds numbers in both laboratory experiments and simulations.

The largest wavenumber for which the inertial subrange spectrum holds may also be determined by dimensional arguments. Dissipation becomes important at the smallest scales, and an additional dimensional quantity, the kinematic viscosity ν, thus enters the scaling. Viscous effects become important at a wavenumber proportional to that which can be formed from ε and ν, with $[\nu] = l^2/t$. Setting the proportionality constant to unity, this wavenumber is called the dissipation wavenumber, and is denoted by

$$k_d = \left(\varepsilon/\nu^3\right)^{\frac{1}{4}} \,. \tag{7.16}$$

The associated length scale is usually denoted as $\eta = k_d^{-1}$. Direct numerical simulations of isotropic turbulence typically show that the energy spectrum starts to deviate substantially from the inertial range law at a wavenumber equal to about one-tenth the dissipation wavenumber k_d.

A self-similar (time-independent) energy spectrum $\widehat{E}(\widehat{k})$ in the inertial and dissipative subranges may now be constructed on dimensional grounds using $\varepsilon = \varepsilon(t)$ and $k_d = k_d(t)$:

$$E(k,t) = (\varepsilon^2/k_d^5)^{1/3}\widehat{E}(\widehat{k})\,; \qquad \widehat{k} = k/k_d\,. \tag{7.17}$$

The three dimensional energy spectrum considered here can be computed by numerical simulation but is difficult to measure directly in physical experiments, where it is more common to present results for the one-dimensional energy spectrum. A self-similar one-dimensional energy spectrum may also be constructed as above, and a compilation of experimental data for the one-dimensional self-similar spectra scaled according to (7.17), Fig. 7.3, shows an excellent collapse at high wavenumbers for a wide range of Reynolds numbers and experimental conditions. The original data for this figure was compiled by Chapman (1979), and has been recently augmented with more recent experimental results by Saddoughi and Veeravalli (1994).

Figure 7.3 demonstrates a universality of small-scale statistics at large Reynolds numbers. Such a universality holds promise for large-eddy simulations, since it implies that the ideas used to develop a subgrid-scale model may have general validity for all turbulent flows, provided of course that the subgrid scales being modeled lie within the universal range of scale sizes made evident in Fig. 7.3.

The concept of local isotropy, which is a part of the Kolomogorov phenomenology, is also an important one. It is based on the idea that, although the largest scales of the flow may be anisotropic due to the presence of boundaries, directional forces, or mean gradients, the smallest scales more closely approach isotropy due to the mixing properties of the nonlinear transfer. The memory of preferred directions in the flow is slowly erased as the energy of the turbulence cascades from large to small scales. The implication of this concept to large-eddy simulation is that one can reasonably develop turbulence models that assume isotropy of the small scales. In a statistical model of the small scales, this will significantly reduce the number of undetermined parameters in the model.

7.3.2 Dissipation set by the large scales

There is another fundamental aspect of turbulence that is also of central importance to the potential success of large-eddy simulations. Arguably the most important formula in all of turbulence modeling is the relation made famous by Batchelor (1953)

$$\varepsilon = u^3/l\,, \tag{7.18}$$

where u and l are a velocity and length scale characteristic of the energy-containing scales of a high Reynolds number, fully turbulent flow. The physical meaning of (7.18) is clear: the energy-containing scales determine the rate of energy dissipation, not the viscous scales. The general validity of (7.18) is of enormous importance for the success of large-eddy simulations: it implies that, if one can capture the largest energy-containing scales of motion with the numerical method, then a

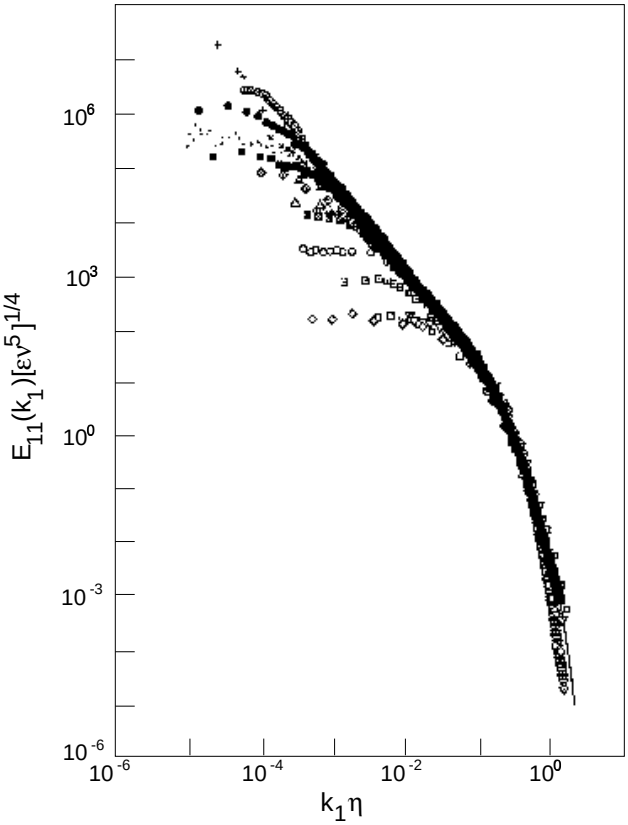

Figure 7.3: Rescaled one-dimensional spectra (from Chapman 1979, with additions from Saddoughi and Veeravalli 1994). The data points represent several experiments in different configurations (grid turbulence, wakes, boundary layers, channels, shear flows, jets) with $23 < Re_\lambda < 3180$.

sophisticated model of the unresolved dissipative scales may be unnecessary, provided that the model for these scales can adjust to the dissipation rate ε set by the largest scales. In other words, relatively crude models of the subgrid scales may work provided they can adapt to the dissipation rate set by the largest scales. This relaxed approach to subgrid scale modelling has found some support among a group of researchers (Oran and Boris 1993) who advocate the use of no explicit subgrid-scale model; rather they let the numerical method itself be dissipative. Dissipative numerical methods, however, have been avoided in the most successful direct numerical simulations of turbulence, where energy-conserving spectral methods have been implemented. Adaptation of these existing codes to large-eddy simulations require explicit subgrid-scale models to dissipate energy at the grid scales.

Related to (7.18) is the idea that the dissipation rate ε approaches a non-zero constant in the limit of zero viscosity (or equivalently, infinite Reynolds numbers). The dissipation rate ε thus must be independent of viscosity at large Reynolds numbers, implying a dependence on large-scale statistics. In a statistically stationary flow, the rate of energy production is equal to the energy flux through the inertial subrange, which is again equal to the dissipation rate. Equation (7.18) implies that it is the rate of energy production that determines the other three.

The fact that the energy spectrum follows a power-law k^{-n} in the inertial subrange, with $n \leq 3$, is of some importance. The energy dissipation rate for isotropic turbulence is given by

$$\varepsilon = 2\nu \int_0^\infty k^2 E(k) dk; \tag{7.19}$$

for an inertial subrange extending to infinite wavenumber, the integral diverges when $n \leq 3$ so that ε need not necessarily vanish with ν.

In fact, using the inertial subrange form for $E(k)$, it is easy to show that (7.19) is not an equation for ε at all, but rather an equation for the Kolmogorov constant Ko. First, one replaces the upper limit of integration by the wavenumber at which dissipation effects become so dominant that the spectrum decays sharply. This wavenumber must be proportional to the dissipation wavenumber k_d, and the proportionality constant is α. It has already been mentioned that dissipation effects are first observed to occur at $0.1k_d$, so that α should be a constant somewhat larger that 0.1. Using the inertial subrange form for $E(k)$ from wavenumber 0 to αk_d, appropriate for very large Reynolds numbers, one finds that the dissipation rate ε and kinematic viscosity ν cancel out of (7.19) after integration, resulting in

$$\mathrm{Ko} = \frac{2}{3\alpha^{\frac{4}{3}}}. \tag{7.20}$$

For values of the Kolmogorov constant $1.4 < \mathrm{Ko} < 2.1$, Eq. (7.20) yields the reasonable values of $0.42 < \alpha < 0.57$. A corollary of this result is that a relatively high Reynolds number DNS need only contain wavenumbers slightly larger than $k_d/2$ to resolve the dissipation range adequately.

7.3.3 Basic requirements of subgrid models

Large-eddy simulations resolve the dissipative scales of turbulence inadequately. In fact, simulations of homogeneous turbulence are often performed with the molecular transport coefficients identically set to zero. In energy-conserving codes, the only way for the turbulence kinetic energy to leave the resolved modes is by the dissipation provided by the subgrid-scale model. Even in large-eddy simulations of bounded flows, which may choose to resolve the wall layer and have non-zero values of the viscosity, the dissipative effects of the molecular viscosity in the interior of the flow may be insufficient, and additional dissipation by the subgrid-scale model is required. Thus, the most important feature of a subgrid-scale model is to provide adequate dissipation. Here, dissipation actually means transport of energy from the resolved grid scales to the unresolved subgrid scales, and the rate of dissipation ε in this context is actually the flux of energy through the inertial subrange.

The subgrid-scale model must not only provide a means of energy dissipation, but the dissipation rate must depend on the large scales of the flow rather than being imposed by the model. Hence, the model must depend on large-scale statistics, and must be sufficiently flexible to adjust to changes in these statistics.

It was once thought by some researchers that the subgrid-scale model should be able to represent explicitely the unknown subgrid-scale stresses (Clark *et al.* 1979). Comparison of modeled subgrid-scale stresses to those calculated from DNS data yielded discouragingly low correlation coefficients. Now, however, it is more widely thought that exact (or even close) representation of the explicit subgrid-scale stresses is an unrealistic goal. The authors' view is that large-eddy simulations are a statistical model of turbulence, and their primary goal is to obtain the correct statistics of the energy-containing scales of motion. This is in contrast to direct numerical simulations, that try to obtain a deterministic solution of the Navier-Stokes equations. Here too, however, the issue of deterministic chaos must be confronted: the sensitive dependence of the evolution of the flow field from its initial conditions makes it meaningless to speak of "following a particular realization of the flow".

If one views large-eddy simulations as statistical models, then one can argue that the subgrid-scale model should also be statistical. This could result in some major simplifications of the model. For statistically steady flows, the subgrid-scale model can be independent of time, or at least a random function of time; for flows with one or more statistically homogeneous directions, the subgrid-scale model can be independent of those spatial directions (or a random function of those directions). In practice, this means that some type of averaging can be performed over time and/or homogeneous directions to determine the free parameters that may appear in the subgrid-scale model. This point will be discussed further when the dynamic subgrid-scale model is presented. It should be pointed out that for flows that are neither statistically steady nor homogeneous, the only averaging available is the ensemble average, that is, an average over multiple individual realizations of the flow.

7.3.4 Eddy viscosity and eddy noise

It is possible to obtain an exact analytical result at high Reynolds numbers for the energy transfer to the subgrid scales defined above in (7.14) from the Navier-Stokes equations, that, although of limited practical use, illuminates the main physics of subgrid-scale modeling. Consider decaying isotropic turbulence. In numerical simulations of this flow, generally, some initial energy spectrum of the turbulence is specified. A velocity field that satisfies continuity, and has the given energy spectrum, is constructed. The Fourier components of this velocity field are typically chosen to have random phases subject to complex conjugate symmetry, as required by the reality of the physical velocity. It is possible to derive exact statistical results for the small-time evolution of this initial field. This is possible because of the following two properties satisfied by the Fourier components with random phases. First, at the initial instant all ensemble-averaged third-order statistics of the velocity field vanish. In particular, the following product of Fourier components is zero at the initial instant:

$$\langle u_l(\vec{k})u_m(\vec{p})u_n(\vec{q})\rangle = 0 \tag{7.21}$$

where $\vec{k}$, $\vec{p}$, and $\vec{q}$ are arbitrary wavenumbers, l, m, and n denote arbitrary components of the velocity field, and $\langle\cdot\rangle$ denotes an ensemble average. Equation (7.21) further implies that the transfer $T(k)$ is identically zero at the initial instant. Second, the velocity field at the initial instant has zero-fourth-order cumulants, so that

$$\begin{aligned}\langle u_l(\vec{k})u_m(\vec{p})u_n(\vec{q})u_s(\vec{r})\rangle &= \langle u_l(\vec{k})u_m(\vec{p})\rangle\langle u_n(\vec{q})u_s(\vec{r})\rangle \\ &+ \langle u_l(\vec{k})u_n(\vec{q})\rangle\langle u_m(\vec{p})u_s(\vec{r})\rangle \\ &+ \langle u_l(\vec{k})u_s(\vec{r})\rangle\langle u_m(\vec{p})u_n(\vec{q})\rangle\,. \end{aligned}\tag{7.22}$$

With zero fourth-order cumulants the usual closure problem of turbulence, in which the equation for an n^{th}-order moment contains unknown terms of $(n+1)^{\text{st}}$-order, is avoided. For isotropic turbulence, the second-order moments may be directly related to the three-dimensional energy spectrum $E(k)$ by

$$\langle u_i(\vec{k})u_j(\vec{k}')\rangle = \frac{P_{ij}(\vec{k})}{4\pi k^2}E(k)\delta(\vec{k}+k'), \tag{7.23}$$

where

$$P_{ij}(\vec{k}) = \delta_{ij} - \frac{k_i k_j}{k^2}\,, \tag{7.24}$$

δ_{ij} is the Kronecker-delta, and $\delta(\vec{k}+k')$ is the Dirac-delta function. For analytical simplicity, here and for the remainder of this Section the limit of infinite periodicity length is assumed, although the numerical simulations commonly choose units in such a way that the periodicity length is 2π.

An exact result to order t may be obtained either by expanding the velocity field as a power series in t, or by forming and integrating the time-evolution equation

for the third-order moments. Both methods involve some tedious algebra, and only the pertinent results are presented here.

The largest wavenumber resolved by the simulation is defined as k_m; the total transfer is then divided into two parts:

$$T(k) = T_{\rm res}(k|k_m) + T_{\rm sub}(k|k_m), \tag{7.25}$$

where the subscript "res" denotes the resolved part of the transfer, and the subscript "sub" the unresolved subgrid part. The transfer consists of an integral over wavenumbers $\vec{p}$ and $\vec{q}$ restricted so that the triangle relation $\vec{k} = \vec{p} + \vec{q}$ is satisfied. The resolved part of the transfer is such that all wavenumber $\vec{p}$ and $\vec{q}$ in the integral also satisfy $p, q \leq k_m$. The unresolved transfer consists of the remaining interactions where one or both of p and q is greater than k_m. This part of the transfer is absent from the LES and its effects on scales of wavenumber $\vec{k}$ must be modeled.

The physical significance of the analytical results is most easily explained under a nonlocal approximation that assumes $k << k_m$. An expansion of the integrands in powers of k/k_m may then be performed that allows a further reduction in the final expression. The result for the subgrid-scale transfer thus obtained is (Lesieur 1990):

$$\begin{aligned} T_{\rm sub}(k|k_m) &= \frac{14}{15}k^4 \int_{k_m}^{\infty} t\frac{E(p)^2}{p^2}dp \\ &- \frac{2}{15}k^2 E(k) \int_{k_m}^{\infty} t\left[5E(p) + p\frac{dE(p)}{dp}\right] dp\,, \end{aligned} \tag{7.26}$$

where the energy spectrum in (7.26) is evaluated at the initial instant.

The second integral on the right-hand side of (7.26) has the form

$$-2\eta(t)k^2E(k) \tag{7.27}$$

where $\eta(t)$ can be called the asymptotic ($k/k_m \to 0$) subgrid-scale eddy-viscosity. For an inertial subrange energy spectrum, η is positive and increases the net viscosity in the large-eddy simulation. The modeling of this term thus provides the means for energy to be dissipated from the resolved scales of the turbulence.

The first integral on the right-hand side of (7.26) is of another form entirely. It is positive, which signifies energy transfer from subgrid to resolved scales. In this nonlocal approximation, it is much smaller in magnitude than the second integral for k_m lying in the inertial subrange. Situations in which this term could be appreciable will be described below.

Equation (7.26) is the leading-order term in an expansion of the subgrid-scale transfer in powers of t. It is thus of limited validity. The more complete, but also approximate, two-point closure theories of turbulence extend the above analytic result to long-time evolutions. For example, in a systematic development of the relatively popular two-point closure model, the so-called eddy-damped quasi-normal Markovian (EDQNM) approximation (Orszag 1970, Lesieur 1990), t is replaced

by a correlation time-scale of the nonlinear interactions among the wavenumber triad $\vec{k}$, $\vec{p}$, and $\vec{q}$, and the energy spectra are evaluated at time t rather than at the initial instant.

The physics of the first integral on the right-hand side of (7.26) may be further elucidated by considering a problem associated with the unpredictability of turbulent flow (Lorenz 1969, Leith 1971, Leith and Kraichnan 1972, Metais and Lesieur 1986, Lesieur 1990). Suppose one performs simultaneously two direct numerical simulations. Both simulations are initialized with the same energy spectrum $E(k)$ for all k. However, in assigning random phases to the initial Fourier components of the velocity field, the same random phases are assigned to Fourier components of wavenumber $k < k_m$ in both simulations, whereas random uncorrelated phases are assigned to the Fourier components with $k > k_m$. An LES with maximum wavenumber k_m corresponding to these two direct numerical simulations would have identical initial velocity fields since the difference between the DNS fields lie in the subgrid scales of the LES. Now, let $u_i(\vec{k},t)$ and $v_i(\vec{k},t)$ be these two distinct velocity fields, identical at $t = 0$ for $k < k_m$ but uncorrelated for $k > k_m$. The difference field $w_i(\vec{k},t)$ can be defined by

$$w_i(\vec{k},t) = \frac{1}{2}\left[u_i(\vec{k},t) - v_i(\vec{k},t)\right], \tag{7.28}$$

and the corresponding error spectrum $E_\Delta(k,t)$ by

$$\langle w_i(\vec{k}) w_j(\vec{k}')\rangle = \frac{P_{ij}(\vec{k})}{4\pi k^2} E_\Delta(k)\delta(\vec{k}+k'). \tag{7.29}$$

At the initial instant, $E_\Delta(k) = 0$ for $k < k_m$ and $E_\Delta(k) = E(k)$ for $k > k_m$. Again, one can tackle this problem analytically as an expansion in t. For $k << k_m$, one finds for the transfer spectrum associated with $E_\Delta(k,t)$,

$$\frac{\partial E_\Delta(k,t)}{\partial t} = \frac{14}{15} k^4 \int_{k_m}^{\infty} t \frac{E(p)^2}{p^2} dp\,. \tag{7.30}$$

The first term of the subgrid-scale transfer in (7.30) thus also appears in this calculation of the error energy transfer. This term has been called eddy noise (Rose 1977), or stochastic backscatter (Leith 1990). A correct model for this term in the filtered Navier-Stokes equations must have a random component since it is responsible for the divergence of two initially identical large-eddy velocity fields with unknown (and hence uncorrelated) realizations of subgrid-scale fields. An analogous eddy noise term is also present in the Navier-Stokes equations themselves (Landau and Lifshitz 1959) due to thermal fluctuations, but is safely neglected due to the wide separation of scales between the molecular and macroscopic motions of the fluid. There is no such large scale separation between the resolved and subgrid fluid elements.

Thus, the two main physical influences of the subgrid-scale motions have been highlighted: eddy viscosity and eddy noise. The former removes energy from the resolved scales of motion in analogy to molecular viscosity, whereas the latter

supplies energy to the resolved scales by some random process. There are two further points worthy of mention. First, so far only the subgrid-scale transfer for $k << k_m$ has been considered. For $k \sim k_m$ the physics of the subgrid-scale transfer are somewhat more complicated. It was shown that the subgrid transfer still divides into an energy input and output term (Kraichnan 1976, Leslie and Quarini 1979). However, both terms are large in magnitude at $k = k_m$, and a cancellation occurs. This cancellation is a consequence of rapid phase changes in the Fourier components near the maximum wavenumber due to the sweeping of small-scale eddies by the largest scales. Random sweeping does not alter energy transfer. The consequences of modeling this random sweeping will be discussed further in Section 7.4.2. Second, it was noted above that for $k << k_m$ and k_m lying in the inertial subrange, the energy input term (eddy noise) is much less than the energy output term (eddy viscosity). However, for k_m lying in the energy-containing scales of motion, or even larger scales, the situation reverses. Although, an ideal LES always has k_m lying in an inertial subrange, this may be impossible for the very important but difficult problems in geophysical turbulence, such as occur in an atmospheric boundary layer (Mason and Thomson 1992). In this work it was claimed that a proper modeling of the energy input term in the subgrid-scale model can significantly improve the LES results.

7.4 Subgrid-scale modeling

7.4.1 Eddy viscosity models

Most subgrid scale models in use presently are eddy-viscosity models of the form

$$\tau_{ij} - \frac{\delta_{ij}}{3}\tau_{kk} = -2\nu_T \overline{S}_{ij}, \tag{7.31}$$

that relate the subgrid-scale stresses τ_{ij} to the large-scale strain-rate tensor

$$\overline{S}_{ij} = \frac{1}{2}\left(\frac{\partial \overline{u}_i}{\partial x_j} + \frac{\partial \overline{u}_j}{\partial x_i}\right). \tag{7.32}$$

In most cases, the eddy viscosity ν_T is obtained algebraically to avoid solving additional equations that could increase the cost of an already expensive calculation. Moreover, since the small scales tend to be more homogeneous and isotropic than the large ones, it is hoped that even simple, algebraic models can describe their physics accurately. Finally, since the SGS stresses only account for a fraction of the total stresses, modeling errors should not affect the overall accuracy of the results as much as in the standard turbulence modeling approach.

There are at least two ways to obtain the eddy viscosity: for homogeneous flows it is convenient to derive it from the Fourier-transformed Navier-Stokes equations (7.11). Another approach is to derive it starting from the SGS energy equation (7.13) in real space. These methods will be discussed in the following.

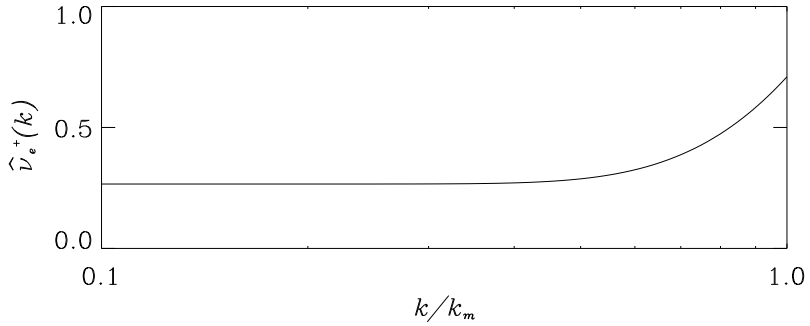

Figure 7.4: Non-dimensional eddy viscosity as parametrized by Chollet (1994).

7.4.2 Modeling in Fourier space

Spectral large-eddy simulations of homogeneous turbulence typically use a subgrid-scale model defined in Fourier space. These models are of limited use in engineering and geophysical applications because of the one or more inhomogeneous directions in these flows. Nevertheless, it is instructive to construct simple models in Fourier space first; they may also be used with great success in studying fundamental problems in turbulence physics without boundaries. The pioneering work in analytically defining and developing a subgrid-scale model in Fourier space was done by Kraichnan (1976). Kraichnan, using a two-point closure model for isotropic turbulence, computed the subgrid-scale transfer $T_{\rm sub}(k|k_m)$ for k_m lying in an infinite inertial subrange. He then defined the following net eddy-viscosity from the calculated subgrid-scale transfer:

$$\nu_e(k|k_m) = -\frac{T_{\rm sub}(k|k_m)}{2k^2 E(k)}. \tag{7.33}$$

Both the contributions from the eddy viscosity and eddy noise (Section 7.3.4) are included in this net eddy viscosity. For k_m lying in the inertial subrange, the net eddy viscosity approaches the k-independent eddy viscosity for $k << k_m$. However, both the eddy viscosity and eddy noise contribute near k_m and the net eddy viscosity increases with increasing k/k_m to a finite cusp at $k/k_m = 1$. Using inertial subrange dimensional arguments, Kraichnan scaled the eddy viscosity using the cascade rate ε, and k_m. The eddy viscosity then becomes proportional to $(\varepsilon/k_m^4)^{1/3}$.

Chollet and Lesieur (1981) soon after proposed a scaling of the eddy viscosity based on the energy spectrum at k_m, and this definition has subsequently found the most use in large-eddy simulations of homogeneous turbulence. The Chollet and Lesieur scaling is

$$\nu_e(k|k_m,t) = \nu_e^+(k/k_m)\sqrt{\frac{E(k_m,t)}{k_m}}, \tag{7.34}$$

so that the eddy viscosity vanishes, as it should, if the subgrid scales contain no

energy ($E(k) = 0$ for $k \geq k_m$). For easy implementation in numerical simulation codes, Chollet (1984) further parametrized the dimensionless eddy viscosity obtained from the EDQNM as

$$\nu_e^+(k/k_m) = \mathrm{Ko}^{-\frac{3}{2}} \left[0.441 + 15.2 \exp\left(-3.03 k_m/k\right)\right] , \tag{7.35}$$

where he chose the Kolmogorov constant to be $\mathrm{Ko} = 1.4$. The Chollet parametrization of the dimensionless eddy viscosity is shown in Fig. 7.4. Note that the eddy viscosity goes to a k-independent constant for $k/k_m << 1$, and rises to a finite cusp at $k/k_m = 1$.

With the eddy viscosity so defined, the LES equations written in Fourier space become

$$\frac{\partial \widehat{u}_i(\vec{k},t)}{\partial t} + \left[\nu + \nu_e(k|k_m,t)\right] k^2 \widehat{u}_i(\vec{k},t) = -ik_n P_{ij}(\vec{k}) \sum_{\substack{\vec{p}+\vec{q}=\vec{k} \\ p\,,q<k_m}} \widehat{u}_n(\vec{p}) \widehat{u}_j(\vec{q}) , \tag{7.36}$$

and it can be observed that this subgrid-scale model is deterministic and strictly dissipative. It is also a statistical model, in the sense that the eddy viscosity depends only on wavenumber magnitude, which is appropriate for isotropic turbulence, and on the energy spectrum $E(k_m,t)$.

The Kraichnan/Chollet-Lesieur eddy viscosity is an easily-implementable k-space subgrid-scale model. It accounts for the missing subgrid-scale transfer by including a parametrized k-dependent eddy viscosity in the equations of motion. Although this eddy viscosity was originally computed using two-point closure theories, it has also been computed directly in a DNS (Domaradzki *et al.* 1987) and in an LES (Lesieur and Rogallo 1989). The DNS results are at too low Reynolds numbers to be directly applicable here, but the LES results demonstrate a reasonable quatitative agreement with the closure theories provided the Kolmogorov constant in (7.35) is taken to be approximately 2.1. The appropriate value of Ko in (7.35) has also been observed to decrease to values in better agreement with experimental data with increasing resolution of the simulations.

It is worthwile to digress a moment to discuss Lesieur and Rogallo's (1989) computation of the subgrid-scale eddy viscosity in an LES. Conceivably, the computation of the subgrid-scale eddy viscosity can be done at each time step in the LES, providing a procedure for the LES to compute its own eddy viscosity. This technique is in the same spirit as the recently-developed dynamic subgrid-scale model, that is beginning to find widespread use in simulations of inhomogeneous turbulence, and which will be discussed in great detail later.

The eddy viscosity can be computed in an LES by introducing another wavenumber k_c such that $k_c < k_m$. A reasonable choice would be $k_c = k_m/2$. The contribution to the transfer $T(k)$ for $k < k_c$ by scales with at least one of p or q in the wavenumber range lying between k_c and k_m may be computed in the LES using fast Fourier transforms (Domaradzki, *et al.* 1987). Denoting this transfer spectrum as $T_{\mathrm{sub}}(k|k_c,k_m)$, the eddy viscosity computed from this restricted transfer

is defined as

$$\nu_e(k|k_c,k_m) = -\frac{T_{\rm sub}(k|k_c,k_m)}{2k^2E(k)}. \tag{7.37}$$

It is desired to make use of this computed eddy viscosity to determine the nondimensional eddy viscosity $\nu_e^+(k/k_m)$ to be used in the simulation at the next time step. The eddy viscosity due to scales with wavenumbers greater than k_c is evidently the sum of the eddy viscosity due to scales with wavenumbers lying between k_c and k_m plus the eddy viscosity due to scales with wavenumber greater than k_m. Hence the relationship between the three eddy viscosities computed with different cutoff wavenumbers is

$$\nu_e(k|k_c) = \nu_e(k|k_c,k_m) + \nu_e(k|k_m). \tag{7.38}$$

This is exactly the Germano identity (Germano 1992) on which the dynamic subgrid-scale model (Germano *et al.* 1991), which will be discussed in Section 7.4.3, is based. Scaling the first and third eddy viscosities as suggested by Chollet and Lesieur, and approximating $\nu_e^+(k/k_m)$ by $\nu_e^+(0)$ (for $k < k_c$, we assume $k << k_m$ so that the eddy viscosity is sufficiently close to its asymptotic value as $k/k_m \to 0$, see Fig. 7.4), one obtains

$$\nu_e^+(k/k_c) = \nu_e(k|k_c,k_m)\sqrt{\frac{k_c}{E(k_c)}} + \nu_e^+(0)\left(\frac{k_c}{k_m}\right)^{\frac{4}{3}}, \tag{7.39}$$

where the last factor in (7.39) comes from assuming inertial subrange forms for the energy spectrum at k_c and k_m. Now it only remains to determine $\nu_e^+(0)$. By considering (7.39) for $k << k_c$ so that $\nu_e^+(k/k_c)$ can be approximated by $\nu_e^+(0)$, and $\nu_e(k|k_c,k_m)$ by $\nu_e(0|k_c,k_m)$, one obtains

$$\nu_e^+(0) = \nu_e(0|k_c,k_m)\sqrt{\frac{k_c}{E(k_c)}}\left[1-\left(\frac{k_c}{k_m}\right)^{\frac{4}{3}}\right]^{-1}. \tag{7.40}$$

This provides the correction to the restricted eddy viscosity that can be computed directly in the LES.

The theoretical idea upon which this whole procedure rests is that the nondimensional eddy viscosity has a universal functional form. This is strictly valid (at least within the closure theories) only if k_m (and k_c) lie in the middle of a lengthy inertial subrange. Of course, if this were true in practice, then one may just as well use directly Chollet's parametrization of the eddy viscosity. Nevertheless, here and in the dynamic subgrid scale model discussed later, it is hoped that the internally-determined eddy viscosity may not be too inaccurate even for k_m close to the energetic scales of motion.

Kraichnan's net eddy viscosity sums the contributions from the eddy viscosity and the eddy noise. A k-space subgrid-scale model has been developed that includes both of these effects separately (Bertoglio 1985, Chasnov 1991a), as suggested by the work of Leslie and Quarini (1979). It was shown that the subgrid-scale transfer may be written as two separate terms:

$$T_{\rm sub}(k|k_m) = -2\eta(k|k_m)k^2E(k) + F(k|k_m)\,. \tag{7.41}$$

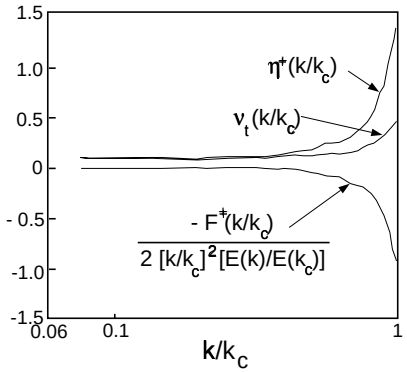

Figure 7.5: Partition of the net eddy viscosity into an eddy-damping term and a stochastic force (from Chasnov 1991a).

This transfer is defined at the statistical level of the turbulence energy equation, and must be de-averaged in order to be modeled at the level of the momentum equations (*i.e.,* the Navier-Stokes equations). The stochastic model form of the EDQNM approximation provides a procedure to accomplish this (Kraichnan 1970): $\eta(k|k_m)$ renormalizes the molecular viscosity, and F is modeled as a random force with zero time correlation. The LES equations thus become

$$\begin{aligned} \frac{\partial u_i(\vec{k},t)}{\partial t} &+ [\nu + \eta(k|k_m,t)]\, k^2 u_i(\vec{k},t) = \\ &- ik_n P_{ij}(\vec{k}) \sum_{\substack{\vec{p}+\vec{q}=\vec{k} \\ p,q<k_m}} u_n(\vec{p}) u_j(\vec{q}) + (\Delta t)^{-\frac{1}{2}} f_i(\vec{k},t)\,, \end{aligned} \tag{7.42}$$

where Δt is the simulation time step, and $f_i(\vec{k},t)$ is constructed independently at each time-step in the same manner in which one constructs an initial velocity field: f_i satisfies continuity, has a spectrum equal to $F(k|k_m)$, and has random phases subject to complex conjugate symmetry. Multiplication by $(\Delta t)^{-1/2}$ is the proper discretization of the white noise process. It allows the stochastic force to provide energy to the turbulence despite having zero correlation with the random velocity field.

Figure 7.5 shows the partition of the net eddy viscosity into an eddy-damping term and a stochastic force. The largest effects of this splitting occur near scale sizes on the order of the grid spacing, *i.e.*, for $k \sim k_m$. Here the effect of the eddy noise is large, and the subgrid model essentially puts energy into these scales by the stochastic force, and takes energy out by the eddy-damping. The net effect is an energy removal represented by the finite cusp of the eddy viscosity. Figure 7.6 shows the results of two simulations of statistically stationary isotropic turbulence. A time average of the normalized energy spectrum $k^{5/3}E(k)/\varepsilon^{2/3}$ is plotted versus k/k_m using either an eddy viscosity model (Fig. 7.6a), or an eddy damping/stochastic force model (Fig. 7.6b). It appears that the inertial subrange

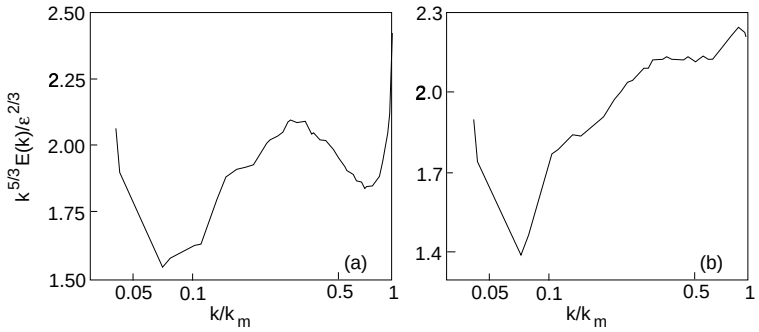

Figure 7.6: Compensated energy spectrum obtained from the large-eddy simulation of a statistically stationary isotropic turbulence (from Chasnov 1991a). (a) eddy viscosity subgrid scale model; (b) eddy damping/stochastic force subgrid scale model.

law is better respected near $k = k_m$ with the second model. This may simply be a consequence of the EDQNM inertial range solution being recovered for $k \sim k_m$, since the individual subgrid-scale terms near the maximum wavenumber are much larger in magnitude than the resolved nonlinear term.

In Section 7.6.1 the results of several large-eddy simulations of homogeneous turbulence will be discusssed further. For most applications, the Kraichnan/Chollet-Lesieur eddy viscosity as parametrized by Chollet (with perhaps some minor tuning) is sufficient to obtain reliable results.

7.4.3 Modeling in real space

The equilibrium assumption

The eddy viscosity is, by dimensional analysis, the product of a length scale, ℓ, and a velocity scale, q_{sgs}. Since the most active of the unresolved scales are those closest to the cutoff, the natural length scale in LES modeling is the filter width, which is the size of the smallest structure in the flow, and is proportional to the grid size. The velocity scale is usually taken to be the square-root of the trace of the SGS stress tensor, $q_{sgs}^2 = \tau_{kk}$. Although in some cases a transport equation is solved to determine q_{sgs}^2, in most cases the equilibrium assumption is made to simplify the problem further and obtain an algebraic model for the eddy viscosity.

The equilibrium assumption is based on the consideration that the small scales of motion have shorter time scales than the large, energy-carrying eddies; thus, it can be hypothesized that they adjust more rapidly than the large scales to perturbations, and recover equilibrium nearly instantaneously. Under this assumption, the transport equation for q_{sgs}^2, (7.13) simplifies significantly, since all terms drop out, except the production term, $\varepsilon_{sgs} = \tau_{ij}\overline{S}_{ij}$, and the viscous dissipation of SGS energy, ε_v, to yield:

$$-\tau_{ij}\overline{S}_{ij} = \varepsilon_v. \tag{7.43}$$

The equilibrium assumption implies inertial range dynamics: energy is generated at the large-scale level, and transmitted to smaller and smaller scales, where the viscous dissipation takes place.

Very little testing of the applicability of this assumption to the small scales of turbulence is available. It is well known that in most flows of interest, the large scales are not in equilibrium: Smith and Yakhot (1993) studied the short-time behavior of the eddy viscosity in the Reynolds-averaged framework, and found that $K-\varepsilon$ models do not predict the correct response of the eddy viscosity if equilibrium turbulence is suddenly subjected to a perturbation (system rotation, for instance). The fact that a SGS model (the Smagorinsky model), applied to the same problem, gave results in good agreement with their theory (Bardina *et al.* 1985), however, indicates that the small scales may tend to equilibrium faster than the large ones, and thus satisfy the equilibrium assumption better than the large scales, or that, as long as the correct non-equilibrium response of the small scales is captured, the overall development of a turbulent flow may be predicted accurately. In more complex flows, in which extra strains, backscatter, intermittency and other phenomena play a role, it is not known whether the small scales would still be represented adequately by equilibrium-based models.

Smagorinsky model

The Smagorinsky model (1963) is, from an historical point of view, the progenitor of all subgrid-scale stress models. It is based on the equilibrium hypothesis, (7.43). If the viscous dissipation is modeled as $\varepsilon \sim q_{sgs}^3/\ell$, and (7.31) is substituted into (7.43) with $\nu_T \sim \ell q_{sgs}$, one obtains $q_{sgs} \sim \ell|\overline{S}|$, where $|\overline{S}| = (2\overline{S}_{ij}\overline{S}_{ij})^{1/2}$ is the magnitude of the strain-rate tensor. Letting $\ell \sim \Delta$, the eddy viscosity can be written

$$\nu_T = (C_s\Delta)^2|\overline{S}|. \tag{7.44}$$

Since the constant C_s (the Smagorinsky constant) is real, the model is absolutely dissipative: $\varepsilon_{sgs} = -(C_s\Delta)^2|\overline{S}|^3 \leq 0$.

To evaluate C_s, Lilly (1967) assumed the existence of an inertial range spectrum $E(k) = \alpha\varepsilon^{2/3}k^{-5/3}$. Then $|\overline{S}|$ can be evaluated approximately by integrating the dissipation spectrum over all resolved wavenumbers

$$|\overline{S}|^2 \simeq 2\int_0^{\pi/\Delta} k^2E(k)dk = 2\alpha\varepsilon^{2/3}\int_0^{\pi/\Delta} k^{1/3}dk = \frac{3}{2}\alpha\varepsilon^{2/3}\left(\frac{\pi}{\Delta}\right)^{4/3}. \tag{7.45}$$

With $\alpha = 1.41$, this gives

$$C_s \simeq \frac{1}{\pi}\left(\frac{2}{3\alpha}\right)^{3/4} = 0.18. \tag{7.46}$$

Dynamic models

In dynamic models for the subgrid-scale stresses, the model coefficients are computed dynamically as the calculation progresses (rather than imposed *a priori*)

based on the energy content of the smallest resolved scale. The dynamic eddy viscosity model of Germano *et al.* (1991) is based on the introduction of two filters; in addition to the *grid* filter (denoted by an overbar), which defines the resolved and subgrid scales, a *test* filter (denoted by a caret)[3] is used, whose width $\widehat{\Delta}$ is larger than the grid filter width $\overline{\Delta}$. The stress terms that appear when the grid filter is applied to the Navier-Stokes equations are the subgrid-scale (SGS) stresses τ_{ij}; in an analogous manner, the test filter defines a new set of stresses, the subtest-scale stresses T_{ij}. The resolved turbulent stresses, $\mathcal{L}_{ij} \equiv \widehat{\overline{u}_i \overline{u}_j} - \widehat{\overline{u}}_i \widehat{\overline{u}}_j$, which represent the contribution of the smallest resolved scales to the Reynolds stresses, can be computed from the large-scale velocity; they are related to the SGS stresses, τ_{ij}, by the identity (Germano 1992)

$$\mathcal{L}_{ij} \equiv T_{ij} - \widehat{\tau}_{ij}, \tag{7.47}$$

where $T_{ij} \equiv \widehat{\overline{u}_i \overline{u}_j} - \widehat{\overline{u}}_i \widehat{\overline{u}}_j$ are the subtest-scale stresses.

The subgrid- and subtest-scale stresses are then parameterized by eddy viscosity models of the form (7.31):

$$\tau_{ij} - \frac{\delta_{ij}}{3}\tau_{kk} = -2C\overline{\Delta}^2 |\overline{S}| \overline{S}_{ij} = -2C\beta_{ij}, \tag{7.48}$$

$$T_{ij} - \frac{\delta_{ij}}{3}T_{kk} = -2C\widehat{\Delta}^2 |\widehat{\overline{S}}| \widehat{\overline{S}}_{ij} = -2C\alpha_{ij}. \tag{7.49}$$

Substituting (7.48) and (7.49) into (7.47) yields

$$\mathcal{L}^a_{ij} = \mathcal{L}_{ij} - \frac{\delta_{ij}}{3}\mathcal{L}_{kk} = -2C\alpha_{ij} + 2\widehat{C\beta_{ij}}. \tag{7.50}$$

This is a set of five independent equations; to obtain a single coefficient from the five independent equations, Lilly (1992), proposed to minimize the sum of the squares of the residual,

$$E_{ij} = \mathcal{L}^a_{ij} + 2C\alpha_{ij} - 2C\widehat{\beta_{ij}}, \tag{7.51}$$

by contracting both sides of (7.50) with $\alpha_{ij} - \widehat{\beta_{ij}}$ to yield:

$$C(\vec{x}, t) = -\frac{1}{2}\frac{\mathcal{L}^a_{ij}(\alpha_{ij} - \widehat{\beta}_{ij})}{(\alpha_{mn} - \widehat{\beta}_{mn})(\alpha_{mn} - \widehat{\beta}_{mn})}. \tag{7.52}$$

This procedure yields a coefficient that is function of space and time, and whose value is determined by the energy content of the smallest resolved scales, rather than input *a priori* as in the standard Smagorinsky (1963) model. The procedure described above, however, is not mathematically self-consistent since it requires that a spatially-dependent coefficient be extracted from a filtering operation

[3] Within the framework of dynamic modeling, a caret does not denote a Fourier coefficient but a test-filtered quantity.

(Cabot and Moin 1993). To overcome this problem, C is usually assumed to be only a function of time and of the spatial coordinates in inhomogeneous directions, and ensemble-averages of the numerator and denominator of (7.52) are taken to yield, for a flow that is statistically-homogeneous in x and z,

$$C(y,t) = -\frac{1}{2}\frac{\langle \mathcal{L}_{ij}^a(\alpha_{ij} - \widehat{\beta}_{ij})\rangle}{\langle(\alpha_{mn} - \widehat{\beta}_{mn})(\alpha_{mn} - \widehat{\beta}_{mn})\rangle}. \tag{7.53}$$

Various methods have been developed to implement a fully localized formulation of the dynamic model that removes the mathematical inconsistency (Ghosal *et al.* 1995, Piomelli and Liu 1995). A one-equation dynamic model including a stochastic backscatter term has also been developed (Ghosal *et al.* 1995, Carati *et al.* 1995).

7.5 Numerical methods

7.5.1 Spatial discretization

The analytical derivative of a complex exponential $f(x) = e^{ikx}$ is $f'(x) = ike^{ikx}$; if f is differentiated numerically, however,the result is

$$\frac{\delta f}{\delta x} = ik'e^{ikx}, \tag{7.54}$$

where k' is the modified wavenumber. A modified wavenumber corresponds to each differencing scheme; the real part of k' represents the attenuation of the computed derivative compared to the actual one, whereas a non-zero imaginary part of k' indicates that phase errors are introduced by the numerical differentiation. For a second-order centered scheme, for instance, $k' = k \sin k\Delta x/k\Delta x$. For small wavenumbers k the numerical derivative is quite accurate; high wavenumber fluctuations, however, are resolved increasingly poorly. No phase errors are introduced. Figure 7.7 shows a sketch of the real part of the modified wavenumbers for various numerical schemes.

The need to resolve accurately high wavenumber turbulent fluctuations implies that either low-order schemes must be used on very fine meshes, or that higher-order schemes are required on coarser meshes. High-order schemes are more expensive, in terms of computational resources, than low-order ones, but the increase in accuracy they afford, for a given mesh, often justifies their use.

Most LES (and DNS) calculations, to date, have been performed using spectral schemes (Fourier expansions in homogeneous directions, Chebychev polynomials in inhomogeneous ones, for instance). These methods are very accurate, but tend to be more expensive than finite-difference schemes, and also give little flexibility in the application of the boundary conditions.

Finite difference schemes, second-order or higher, are also being used with increasing frequency. As the application of LES is shifting from basic, building-block

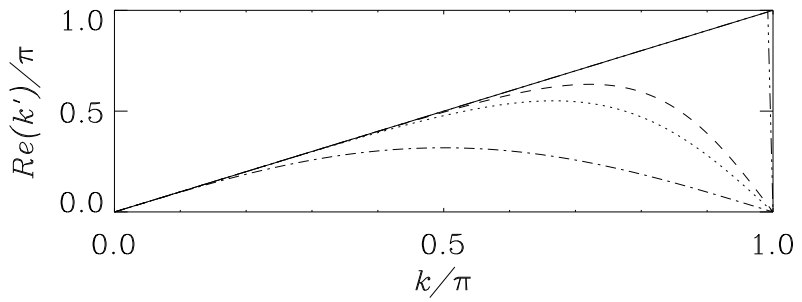

Figure 7.7: Modified wavenumber for various numerical schemes. —— Exact; —·— second-order central; ····· fourth-order compact; - - - fourth-order Padè; —···— spectral.

flows in simple geometries towards more realistic applications, however, the additional flexibility that finite differences enjoy in the treatment of complex geometries and boundary conditions is resulting in their more widespread application.

7.5.2 Time advancement

The choice of time advancement method is usually determined by the requirements that numerical stability be assured and that the turbulent motions be accurately resolved in time. Two stability limits apply to LES calculations. The first is the viscous condition, that requires that the timestep Δt be less than $\Delta t_v = \sigma \Delta y^2/\nu$ (where σ depends on the actual time advancement chosen; for implicit schemes, $\sigma = \infty$). The CFL condition requires that Δt be less than $\Delta t_c = \mathrm{CFL}\Delta x/u$, where the maximum allowable Courant number CFL also depends on the numerical scheme used. Finally, the physical constraint requires Δt to be less than the time scale of the smallest resolved scale of motion, $\tau \sim \Delta x/U_c$ (where U_c is a convective velocity).

In most flows, the viscous condition demands a much smaller timestep than the other two; for this reason, the diffusive terms of the governing equations are usually advanced using implicit schemes (typically, the second-order Crank-Nicolson scheme). Since, however, $\Delta t_c \simeq \tau$ (usually, they differ by a factor of 3 to 6), the convective term can be advanced by explicit schemes such as the second-order Adams-Bashforth method, or third- or fourth-order Runge-Kutta schemes. In compressible flow calculations, or in unbounded flows in which the mesh must not be very fine near a solid surface, fully explicit schemes are often employed.

7.5.3 Boundary conditions

Associated with the widespread use of Fourier methods in LES is the adoption of periodic boundary conditions. Periodic boundary conditions imply that the computational domain repeats itself an infinite number of times, or that the flow is fully developed and statistically steady in space. Periodic boundary conditions

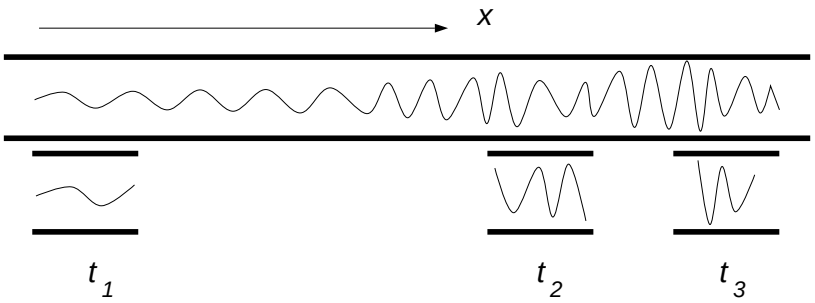

Figure 7.8: Evolution of perturbations in a channel: spatial *vs.* temporal development.

are convenient, since they eliminate the need to specify inflow conditions, easy to implement (in fact they are applied implicitly by Fourier methods) and efficient, since they allow use of small computational domains.

The use of periodic boundary conditions is similar to studying the time development, rather than the spatial development, of a flow; if one looks at the spatial evolution of a perturbation in plane channel (Fig. 7.8), for instance, the use of periodic boundary conditions is equivalent to studying the flow in a convecting frame of reference. Each flow realization (*i.e.*, each timestep) is then equivalent to one location in the spatially-developing framework.

When periodic boundary conditions are used, the computational domain must be at least as long as the wavelength of the longest structure present in the flow. If such wavelength is not known *a priori*, the two-point correlations must be examined to determine whether the domain length is sufficient.

If the flow is spatially developing, it is necessary to specify inflow and outflow conditions. The specification of inflow conditions is straightforward for transitional flows, not so for turbulent flows. In all cases an entire plane of data (all velocity components) must be assigned at each instant. In transitional flows it is sufficient to specify the mean flow and the desired perturbations. For fully-developed turbulent flows one can use the same technique, but the length required for the disturbance to develop and for the flow to reach the desired turbulent state may be very significant, even if large-amplitude perturbations or random noise are given at the inflow. Alternately, one can superpose a turbulent mean flow and random noise with assigned second (or higher) moments. This approach is more physical, and requires shortened adjustment lengths, but semi-empirical information is needed to specify the inflow profiles desired. Finally, one can use the results of a periodic simulation as inflow for a non-periodic one. For instance, one can compute a turbulent channel flow and store, at each timestep, one plane, which is then used as inflow condition for the calculation of a backward facing step. Outflow boundary conditions are usually implemented through a buffer region in which the equations are parabolized (see, for example, Street and Macaraeg 1989).

An alternative approach, developed to allow the application of periodic boundary conditions in spatially-developing flows is the "fringe method" (Spalart and

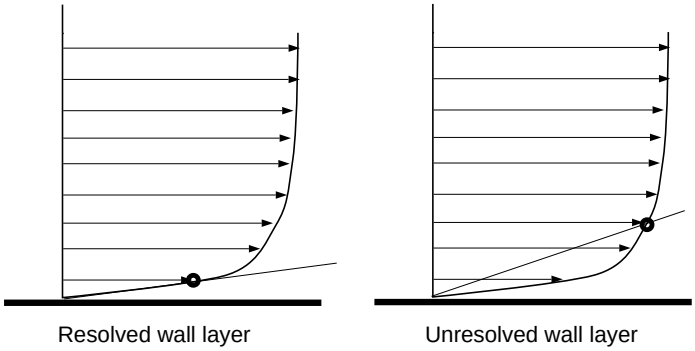

Figure 7.9: Stress at the wall.

Watmuff 1993), in which sink terms are added to the governing equations in a buffer region at the end of the domain. The purpose of these additional terms is to decrease the boundary layer thickness and, if necessary, to accelerate the decay of particular fluctuating components. These terms are active only in a small region (usually, about one quarter of the length of the computational domain), and the Navier-Stokes equations are solved everywhere else.

At solid boundaries, the momentum flux through the boundary must be known. Since the wall velocity is assigned, the no-slip condition allows the determination of the convective part $u_i u_n$ (where a subscript n indicates the direction normal to the boundary) of the momentum flux at the wall. Differentiation of the velocity profile to determine the viscous part, however, is accurate only if the wall-layer is well-resolved. To represent accurately the structures in the near-wall region, the first grid point must be located at $y^+ < 2$,[4] Fig. 7.9, and the grid spacing must be of order $\Delta x^+ \simeq 50 - 150$, $\Delta z^+ \simeq 15 - 40$. As $Re \to \infty$, an increasing number of grid points must be used to resolve a layer of decreasing thickness. This may also result in high aspect-ratio cells, with further degradation of the numerical accuracy.

When the grid is not fine enough to resolve the near-wall gradients, the momentum flux through the wall cannot be evaluated directly by numerical differentiation; the wall layer must then be modeled by specifying a correlation between the velocity in the outer flow and the stress at the wall. This approach allows the first grid point to be located at $y^+ \simeq 30 - 150$, and, since the energy-producing vortical structures in the wall-layer do not have to be resolved, it permits the use of coarser meshes in the other directions as well: $\Delta x^+ \simeq 100 - 600$, $\Delta z^+ \simeq 100 - 300$. Since modeling of the wall-layer physics is required, further empiricisms are introduced in the calculations

[4] A superscript + indicates quantities normalized by the viscosity ν and the friction velocity $u_\tau = (\tau_w/\rho)^{1/2}$.

7.5.4 Initial conditions

For flows that are statistically steady, the initial conditions are relatively unimportant. Usually, they may consist of large-amplitude perturbations superposed on a realistic mean flow, or of a fully-developed flow in a similar configuration. Typically, the flow is allowed to develop in time until a steady state is reached, and then statistics are accumulated.

For flows in which the transient is important (temporal transition, for instance, or the decay of homogeneous isotropic turbulence), more care must be used when assigning the initial conditions. In problems involving laminar-turbulent transition, controlled or random perturbations can be used. For turbulent flow problems, on the other hand, assigning random noise with a given spectrum requires some adjustment time before the nonlinear interactions become realistic.

7.5.5 Implementation on parallel computers

More and more institutions are acquiring parallel computers for high performance scientific computation. The cost of these machines per megaflop may be as little as one-tenth the cost of the more traditional supercomputers, so that small to mid-range versions of these new machines can be directly purchased by individual Universities and corporations. High-end versions of these parallel machines, by definition, are still expensive but can achieve levels of performance unattainable by the more traditional serial machines.

The main challenge confronting the turbulence simulator with these new machines consists in developing a numerical procedure for time-integrating the Navier-Stokes equatins in parallel. The main ideas involved in the implementation of a periodic, spectral turbulence simulation on a parallel machine (Wray and Rogallo 1992) will be discussed here. Developments along similar lines may also be found in Karniadakis and Orszag (1993).

The periodic spectral code time-advances the velocity field in three-dimensional Fourier space. In the original and simplest version of the code, the data structure of the Fourier-transformed velocity field is such that x-y planes of data are distributed uniformly among the P processors. In other words, for a given value of k_z, all the data for k_x and k_y resides locally on each processor. If one is performing a 256^3 simulation, for instance, on 128 processors, then each processor will have data corresponding to two distinct values of k_z. This is what Rogallo has called the *planes code*. The main computational burden in the so-called pseudo-spectral method for solving the Navier-Stokes equations (Orszag and Patterson 1972) is in the fast Fourier transforms between wave-space and physical space used to compute the nonlinear terms as local products rather than as convolutions. Wray and Rogallo (1992) chose to implement these Fourier transforms locally on each processor. With the k_z data spread among processors, only transforms in x and y can be performed locally. The transform in z can be done only after the data has been transposed, that is, the k_z data is swapped with the k_y data, say, so that $k_x - k_z$ planes are local to each processor. The data flow of the code used to

compute the non-linear products is the following: the simulation is initialized in wavespace with $k_x - k_y$ planes local to each processor. First, the velocity field is Fourier-transformed to physical y space. The field is then transposed so that $k_x - k_z$ planes are processor-local. The remaining two transforms are then performed so that the field resides entirely in physical space, the nonlinear terms are formed, and the field is transformed back to wave x and z space. The field is transposed again, transformed to wave y space, and time-advanced. The data management in the planes code is relatively simple and efficient. However, mainly looking ahead to massively parallel machines with a large number of processors (some current machines now contain thousands of relatively slow processors), Rogallo has implemented a more sophisticated version of parallel code that he calls the *pencil code*. The problem with the planes code on massively parallel machines (more than 1000 processors) is that reasonably-sized simulations cannot make use of all the processors. With the pencil code, N^2 modes are mapped onto P processors. Hence, only data in one direction is local to a processor, while data in the other two directions is distributed among the P processors. The data flow is slightly more complicated with the requirement of several transposes. Execution of the pencil code is also somewhat slower than that of the planes code.

Another obvious approach to turbulence simulation on parallel machines is to replace the one large simulation by an ensemble of smaller sized simulations. This has been done using a version of Rogallo's planes code in order to obtain good statistics of the largest scales of isotropic turbulence (Chasnov 1993). In this work, sixty-four 64^3 independent simulations were run in parallel on 128 processors of a parallel machine. Each 64^3 simulation required the memory of two processors to run. When each simulation can fit on one processor, such simulations are called embarrassingly parallel, since little or no communication is required among different processors. The simultaneous running of a large ensemble of flows is an entirely plausible route for the future of LES on parallel machines since the resolution requirements tend to be lower than for DNS, whereas convergence of the large-scale statistics typically require either long time averages (if the flow is statistically steady) or an average over a large ensemble of statistically independent flows.

7.6 Applications

7.6.1 Homogeneous turbulence

A turbulent flow is *homogeneous* if the statistics of the flow are invariant under translation. It is *isotropic* if the statistics are also invariant under rotation. There are no special positions in homogeneous turbulence, and there are no special directions in isotropic turbulence. Isotropic turbulence is necessarily homogeneous (two distinguishable points form a line, and hence specify a direction), but homogeneous turbulence need not be isotropic. The study of homogeneous turbulence excludes all wall bounded flows, since the distance from the wall naturally distinguishes one point in space from another. Some limited physics can be studied

within the framework of isotropic turbulence, including the transport of isotropic passive scalar and magnetic vector fields. However, more interesting physics can be studied within the larger framework of homogeneous turbulence, including the effects of buoyancy, stratification, rotation, external magnetic fields and shear. All these flows are anisotropic in that preferred directions exist (*e.g.*, gravity defines the vertical direction).

This Section will mainly concentrate on two issues concerning homogeneous turbulence. First, the feasibility of LES will be directly tested; that is, an LES of decaying isotropic turbulence will be performed in an attempt to judge the accuracy of the numerical results. Then, following this necessary preliminary discussion which hopefully will serve the purpose of "field testing" LES, the emphasis will switch to the physics of the homogeneous turbulence decay. In particular, some recent LES results will be reviewed that demonstrate precisely the development of asymptotic similarity states in a variety of homogeneous turbulence flows.

One use of homogeneous turbulence simulations has been to test the performance of newly-developed subgrid-scale models. It is reasonable to insist that newly-developed models perform well for simulations of homogeneous turbulence if one is to have any confidence in their use in more complicated geometries. How does one judge the accuracy of an LES? One approach is to simulate decaying grid turbulence, and to compare the results of the LES to physical experiments (Lund *et al.* 1993). The main technical difficulty in this approach is in exactly matching the initial conditions of the simulation to that of the experiment. Another "difficulty" is the observed insensitivity of the large-scale statistics of decaying isotropic turbulence to changes in the subgrid-scale model. However, this perceived difficulty is actually a positive feature, since the robustness of the large-scale statistics of homogeneous turbulence to changes in the subgrid scale model provides evidence that the large-eddy simulations are producing the correct results. Intuitively, one expects incorrect results to be sensitive to changes in the subgrid-scale model which is after all the cause of these incorrect results.

Here, the performance of the k-dependent eddy viscosity subgrid scale model, discussed in Section 7.4.2, will be studied for the fundamental problem of decaying isotropic turbulence at high Reynolds numbers (the molecular transport coefficient will be set to zero in the simulations). Rather than comparing the numerical results to physical grid turbulence experiments, the robustness of the large-eddy statistical results to substantial changes in the subgrid-scale model will be tested directly. The simulations are initialized with a given energy spectrum, and the initial velocity field corresponding to this energy spectrum is constructed using random phases as described earlier. Results of two separate tests of the k-dependent eddy viscosity subgrid-scale model will be presented. First, the results of two large-eddy simulations with identical initial energy spectra but different resolutions of the smallest scales will be compared. In other words, with a fixed initial spectrum the results of two simulations at resolutions 128^3 and 256^3, with maximum resolved wavenumber magnitudes 60 and 120, respectively, will be compared. The minimum wavenumber magnitude is unity. The initial energy spectrum is chosen

to be

$$E(k,0) = \frac{2}{\sqrt{\pi}} u_0^2 k_p^{-1} (k/k_p)^2 \exp\left[-(k/k_p)^2\right], \tag{7.55}$$

with a maximum value at $k_p = 50$. The value of u_0 is unimportant and it is taken to be $u_0 = 1$. The time-evolution of the large-scale statistics of the mean-square velocity of the turbulence, the integral scale, and the energy spectrum itself will be considered. The choice of $E(k,0) \sim k^2$ as $k \to 0$ necessarily results in energy spectra that are the same for all times at small wavenumbers. The physical consequences of this will be discussed in greater detail later.

In decaying turbulence, the integral scale is growing in time so that the dissipation provided by the subgrid-scale eddy viscosity at a fixed resolved wavenumber k is decreasing relative to the resolved scale nonlinear transfer at k. Accordingly, one expects more accurate results after long time evolutions. However, the errors in the results at short times can conceivably pollute the results at later times. Also, in the 256^3 simulations the dissipation provided by the eddy viscosity at k is less than that provided in the 128^3 simulation so that one expects the 256^3 calculation to be more accurate. The dissipation integrated over all k, however, needs to be the same for the two simulations to yield identical results. The integrated dissipation is just the cascade rate ε:

$$\varepsilon(t) = \int_0^{k_m} 2\nu_e(k|k_m,t) k^2 E(k,t) dk \,. \tag{7.56}$$

The results of the 128^3 and 256^3 simulations are shown in Fig. 7.10. In Fig. 7.10, the time-evolution of the mean-square velocity $\langle \mathbf{u}^2 \rangle$ is displayed. Time is in units of the initial large-eddy turnover time $\tau_0 = L_0/u_0$, where L_0, the initial integral scale, is given by $L_0 = \sqrt{\pi}/k_p$. At the initial instant, $\langle \mathbf{u}^2 \rangle = u_0^2$ where $u_0 = 1$. Note that the mean-square velocity statistic is not completely resolved at the initial instant in the 128^3 resolution simulation. Nevertheless, the mean-square velocity statistic from the two simulations converge at the latest times, indicating the successful long-time calculation of this statistic. The time-evolution of the spherically-averaged integral scale is plotted in Fig.. 7.10b. Again, this statistic is not entirely resolved at the initial instant in the 128^3 simulation, but the results from the two simulations converge at the latest times. The initial energy spectrum of the 256^3 simulation, and the final energy spectra from the 128^3 and 256^3 simulations at the nondimensional time of $t/\tau_0 = 300$ are shown in Fig. 7.10c. The agreement of the energy-containing scales of motion at this late time is remarkable. The small-scale spectra do not agree as well, but their disagreement yields the same integrated value for the mean-square velocity.

As a second test of the LES, the evolution of decaying isotropic turbulence at 128^3 resolution, but with significantly modified subgrid-scale models is further considered. The perturbation to the subgrid-scale eddy viscosity is accomplished by assuming the Chollet form for the subgrid-scale model (7.35) with Ko = 2.1, and multiplying it by an extra factor α:

$$\nu_e^+(k/k_m) = \alpha \left[0.145 + 5.01 \exp\left(-3.03 k_m/k\right)\right] . \tag{7.57}$$

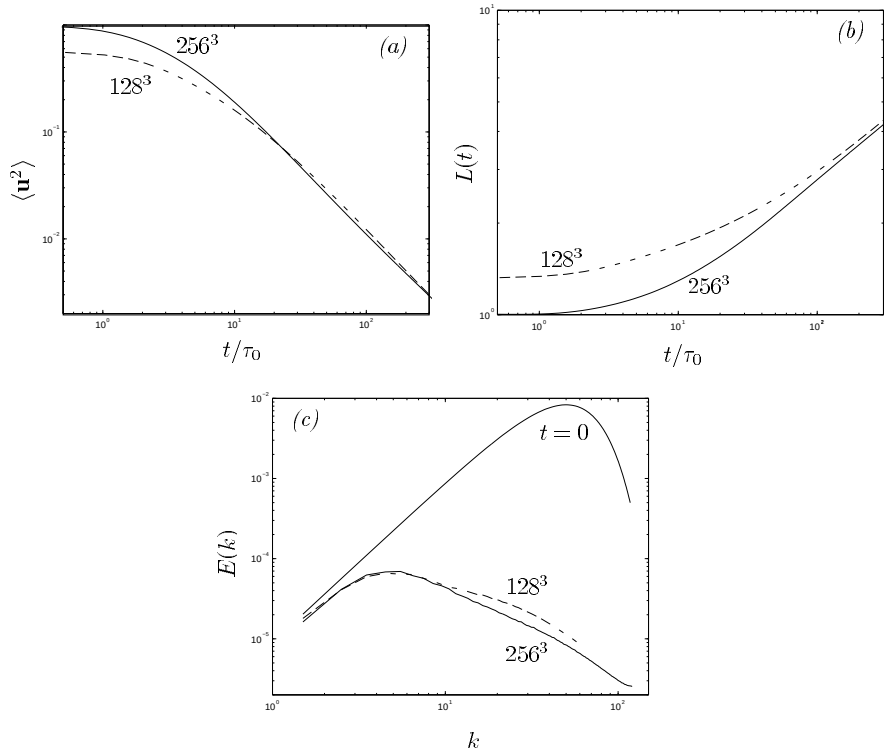

Figure 7.10: The results of 128^3 and 256^3 simulations using a k-dependent eddy viscosity. (a) $\langle \mathbf{u}^2 \rangle$ *vs.* t/τ_0; (b) $L(t)$ *vs.* t/τ_0; (c) Energy spectra at $t/\tau_0 = 300$.

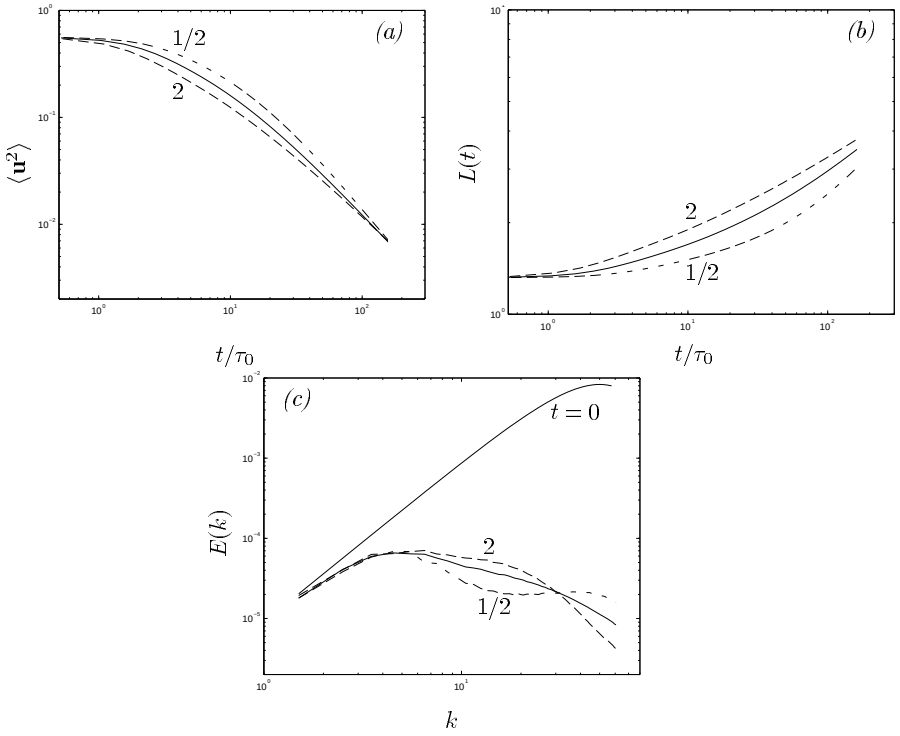

Figure 7.11: The results of 128^3 simulations with perturbed k-dependent eddy viscosity ($\alpha = 1/2$, 1, and 2 in (7.57). (a) $\langle \mathbf{u}^2 \rangle$ *vs.* t/τ_0; (b) $L(t)$ *vs.* t/τ_0; (c) Energy spectra at $t/\tau_0 = 300$.

Consider the evolution of the turbulence with $\alpha = 1/2$, 1, and 2 (in the computations just discussed, α had been taken to be unity). Note that the initial energy dissipation rate of the turbulence varies over a factor of 4 as α varies from 1/2 to 2.

The statistical results are shown in Fig. 7.11. Mean-square velocities and integral scales agree exactly at the initial instant of time, disagree somewhat at intermediate times, and then reconverge at the latest times. The energy spectra at the initial and latest time ($t/\tau_0 = 300$) are displayed in Fig. 7.11. The maximum value attained by the energy spectrum agrees in these three simulations, but significant differences exist for the spectrum of the small scales: the spectrum with $\alpha = 1$ appears to be the most natural with respect to the development of a Kolomogorov inertial subrange (see Section 7.3.1). The main point these results highlight is that, although the spectral distribution of the energy is sensitive to the precise form of the subgrid-scale model, the integral of the spectrum, which yields one-half the mean-square velocity, is not. The turbulent flow apparently self-adjusts to errors in the subgrid-scale model in order to yield the correct energy dissipation rate. This has been picturesquely called "a convenient conspiracy"

(Oran and Boris 1993). One may further attempt to develop subgrid-scale models (or even tune the parameters in the Chollet parametrization) to yield results in better agreement with the Kolmogorov inertial subrange. One method to do this, discussed in Section 7.4.2, requires the addition of a stochastic force. However, results that are sensitive to the subgrid-scale model must be viewed somewhat warily.

Having thus demonstrated the reliability of large-eddy simulations for computing the mean-square velocity and integral scale, some recent results obtained by LES for the development of high Reynolds number similarity states in decaying homogeneous turbulence will be reviewed. The establishment of similarity states in homogeneous turbulence is certainly of theoretical interest: a substantial reduction in the number of independent variables is possible if turbulence is found to decay self-similarly. In fact, it will be shown that the evolution of some non-trivial homogeneous turbulent flows may be predicted by simple dimensional arguments, and that these predictions have been verified to high precision by large-eddy simulations. One can even argue that the "turbulence problem" is solved for these flows in that one can predict exactly their asymptotic statistical evolution. Unfortunately, these types of similarity states may be peculiar to homogeneous turbulence decay in an infinite fluid; nevertheless, the insight gained in studying homogeneous turbulence subject to additional physics such as stable-stratification and rotation may eventually find use in the development of better turbulence models for wider application in engineering and the physical sciences. At least, it will be demonstrated that real progress is possible in turbulence prediction, even if only for idealized situations.

Large-eddy simulations – used to discover new similarity states in homogeneous turbulence and to test theoretical predictions – appears to be uniquely suited to this problem: the long-time evolution of the energy and integral scales characteristic of the asymptotic similarity states is insensitive to the exact form of the subgrid-scale model (as demonstrated above for decaying isotropic turbulence), and alternative approaches such as physical experiments and direct numerical simulations are too severely restricted in Reynolds numbers and total flow evolution time to definitively attain the asymptotic state. Closure calculations of turbulence can attain the high Reynolds numbers and long-time evolutions required (Lesieur 1990), but contain unknown errors that cannot be easily quantified. Furthermore, closure calculations are much more difficult to develop and apply to anisotropic flows than LES. For most problems, an isotropic LES code is easily modified to include additional physics (buoyancy, stratification, rotation, magnetic fields) that may induce anisotropy in the flow field. Closure theories (and the non-trivial numerical codes to solve them) typically require major new developments (Cambon *et al* 1981, Cambon and Jacquin 1989) to include the effects of various anisotropy-producing physics.

Some early applications of LES to homogeneous turbulence will now be briefly reviewed. One of the first LES of forced isotropic turbulence used an empirically-determined eddy-viscosity subgrid-scale model (Siggia and Patterson 1978). Decaying turbulence simulations (Chollet and Lesieur 1981) using an eddy viscosity

subgrid-scale model derived from two-point closure studies (Kraichnan 1976) were later performed with the same spectral code. These early simulations were at the relatively low resolution of 32^3. It is in fact not possible to obtain similarity states for the decaying turbulence at these resolutions since the integral scale grows to a length comparable to the periodic box before a similarity state is attained.

Simulations at the higher resolution of 128^3 that included transport of passive scalars (Lesieur and Rogallo 1989) were undertaken using an isotropic turbulence code developed earlier by Rogallo (1981). Although the decay exponent of the kinetic energy was in qualitative agreement with the theoretical predictions, these simulations yielded some puzzling results for the passive scalar evolution, including a much more rapid decay of scalar variance than was predicted by two-point closure studies (Larcheveque *et al.* 1980). These two-point closure studies were motivated by experimental results obtained from measurements of decaying passive scalar fluctuations in grid-generated turbulence (Warhaft and Lumley 1978). In these experiments, it was determined that the decay exponent of the passive scalar was a function of the ratio between the initial integral length scales of the velocity and scalar fluctuations. Although two-point closure studies seemed to explain this non-universality of the decay exponent as a transient response of the scalar field, the LES results of Lesieur and Rogallo (1989) seemed to be in direct contradiction to the two-point closure results. Further calculations by Metais and Lesieur (1992) seemed to confirm these new LES results.

However, Chasnov (1994) later demonstrated, by placing the peak of the initial energy spectrum at larger wavenumbers, that the anomalous results obtained by Lesieur and Rogallo (1989) for the passive scalar decay were a consequence of too short a time evolution of the flow field. This had been previously suggested by Herring (1990) based on additional two-point closure studies. The Lesieur and Rogallo (1989) results, although certainly accurate, were indeed transient results. These transients may last up to 500 initial large-eddy turnover times of the turbulence, which corresponds to approximately 15 intrinsic large-eddy turnover times of the flow, since the large-eddy turnover time increases as the flow evolves due to the decaying velocity fluctuations and increasing integral scale. Large-eddy simulations also demonstrated that these transients depended on the initial ratio between the velocity and scalar integral scales, as shown earlier by the experiments.

Although it is not the purpose of this article to go into the details of the theoretical scaling laws, it is worthwhile to discuss briefly these analytic results for the simplest case of isotropic turbulence decay so that the LES results can be better appreciated. Theoretical arguments by Batchelor and Proudman (1956) and later by Saffman (1967a) explicitly determined the following low wavenumber ($k \to 0$) forms of the energy spectrum in isotropic turbulence:

$$E(k) \sim 2\pi k^2 B_0 \,, \quad \text{or} \quad E(k) \sim 2\pi k^4 B_2 \,, \tag{7.58}$$

depending on the conditions of turbulence generation. Although the Saffman k^2 form appears to be the generic form, grid turbulence experimental results have mainly supported the Batchelor and Proudman k^4 form by indirect measurements of the velocity decay. Large-eddy simulations discussed here can shed no light on

the experimental large-scale structure of turbulence since it will be shown below that the form of the low wavenumber spectrum is simply determined by the choice of initial conditions in the simulation.

Saffman showed analytically that the low wavenumber coefficient B_0 is an invariant of the flow. If it is initially non-zero, he further postulated a similarity state of the turbulence decay based on B_0 (Saffman 1967b). This similarity state results in the following predictions for the decay of the mean-square velocity and growth of the turbulence integral scale, obtained by simple dimensional analysis:

$$\langle \mathbf{u}^2 \rangle \propto B_0^{2/5} t^{-6/5}\,, \quad L \propto B_0^{1/5} t^{2/5}\,. \tag{7.59}$$

Using these laws, the asymptotic similarity state of the energy spectrum is thus given by

$$E(k,t) = B_0^{3/5} t^{-4/5} \widehat{E}(\widehat{k})\,, \quad \widehat{k} = B_0^{1/5} t^{2/5} k\,. \tag{7.60}$$

Note the reduction of the two independent variables in the spectrum $E(k,t)$ to the one indendendent variable of the similarity spectrum $\widehat{E}(\widehat{k})$.

If the initial turbulence spectrum has B_0 equal to 0, then a non-zero value of B_2 is necessarily generated by nonlinear transfer processes (Batchelor and Proudman 1956). Hence, simulations initialized with a k^2 energy spectral form at low wavenumbers maintain this k^2 form for all times, whereas simulations initialized with energy spectral forms steeper than or equal to k^4 at low wavenumbers subsequently develop a k^4 form. Apparently, a similarity state can also be based on the coefficient B_2 even though it is a function of time. This similarity state was first postulated by Kolmogorov (Kolmogorov 1941) based on the assumption that B_2 was invariant (Loitsianskii 1939). The development of the mean-square velocity and integral scale in this similarity state is given by

$$\langle \mathbf{u}^2 \rangle \propto B_2^{2/7} t^{-10/7}\,, \quad L \propto B_2^{1/7} t^{2/7}\,; \tag{7.61}$$

and the corresponding asymptotic similarity spectrum by

$$E(k,t) = B_2^{3/7} t^{-8/7} \widehat{E}(\widehat{k})\,, \quad \widehat{k} = B_2^{1/7} t^{2/7} k\,. \tag{7.62}$$

Further details of the large-eddy simulations of decaying isotropic turbulence and passive scalar field (Chasnov 1994) will now be discussed. The Chollet parametrization of the eddy-viscosity, [Eqs. (7.34) and (7.35) with Ko = 2.1] is assumed for the subgrid-scale model, and an eddy-diffusivity for the scalar field is defined as

$$D_e(k|k_m,t) = \nu_e(k|k_m,t)/\sigma_e\,, \tag{7.63}$$

where σ_e is an eddy Schmidt (or Prandtl) number, assumed constant and equal to 0.6. Equation (7.63) is a crude but adequate approximation of results obtained from two-point closure models for passive scalar transport. The time-evolution of the energy spectrum for both k^2 and k^4 initial conditions is shown in Fig. 7.12. The peak of the initial spectrum is placed at a wavenumber $k = 100$, where the maximum wavenumber of the simulation is approximately 120 and the minimum

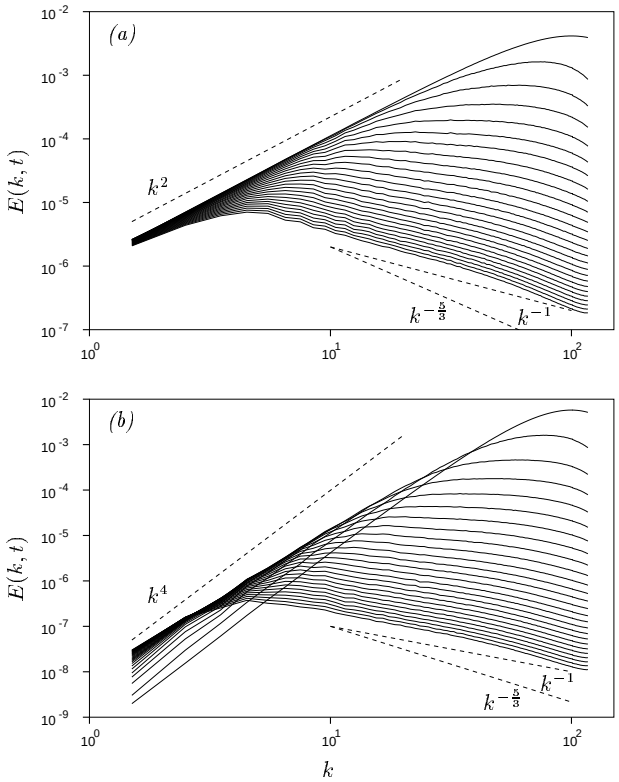

Figure 7.12: Time evolution of the energy spectrum of decaying isotropic turbulence (from Chasnov 1994). (a) k^2 low wavenumber spectrum; (b) k^4 low wavenumber spectrum.

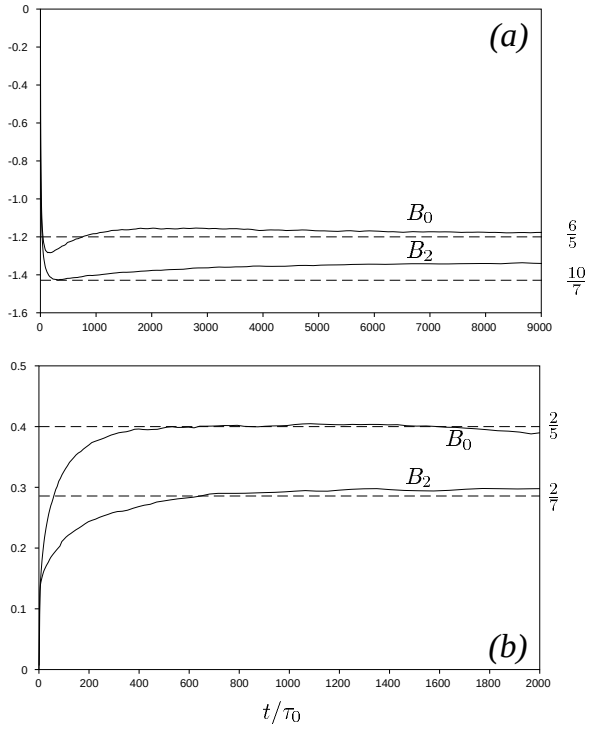

Figure 7.13: Time evolution of the power-law exponent of the mean-square velocity and integral scale of decaying isotropic turbulence. The solid lines are the results of the large-eddy simulations, and the dashed lines are the exact and approximate theoretical results discussed in the text (from Chasnov 1994). (a) Power-law exponent of $\langle \mathbf{u}^2 \rangle$; (b) Power-law exponent of $L(t)$.

wavenumber is unity. These simulations use 256^3 grid points and were performed using a parallel version of the Rogallo code (Wray and Rogallo 1992). The initial flow field is truly a large-eddy field, with even the energy containing scales of motion marginally resolved. As already observed in the first half of this Section, the initial evolution of the large-scale statistics of the flow is in error, but accuracy is recovered after a sufficiently long time evolution. Placing the peak of the initial spectra at such a large wavenumber allows a sufficiently long time evolution of the flow so that the sought-after asymptotic similarity state can be attained before the integral scales of the flow become comparable to the periodicity length of the calculation.

Figure 7.13 displays the time-evolution of the power-law exponent of the mean square velocity and integral scale of the turbulence. Excellent agreement with the theoretical results discussed previously is obtained after a sufficiently long time. Indeed, the Saffman $-6/5$ theoretical result for the time exponent of the mean-square velocity is confirmed to within 2%. A collapse of the energy spectra in

self-similar variables was also explicitly demonstrated by the LES results. Comparatively precise results were also obtained for the passive scalar decay in this work.

It is quite amazing that this type of precision is currently obtainable from large-eddy simulations. To demonstrate this point further, the additional simulations performed by Chasnov (1993) to compute the time-variation of the Loitsianskii integral B_2 in order to provide a correction to the original Kolmogorov $-10/7$ decay exponent should be mentioned. Chasnov (1993) obtained an estimate for the correction to the Kolmogorov decay exponent on the order of 5%; that is, the Kolomogorov $-10/7 \approx -1.43$ time exponent was shown to become approximately -1.36 if the time dependence of B_2 (found to increase as $t^{0.25}$) was accounted for. This should be compared to previous EDQNM results of -1.38 (Lesieur and Schertzer 1980). These simulations, however, were fairly expensive at the time, requiring the computation of an ensemble of 1024 realizations of 64^3 flows. However, with the rapid increase in the projected speed and memory of parallel computers, these computations may appear inexpensive to the present reader.

How does LES perform for anisotropic turbulence? The decay of an initially-axisymmetric turbulence was recently investigated using LES (Chasnov 1995a). Following the theoretical work of Saffman (1967a), initial conditions corresponding to impulsive forces along and perpendicular to the axis of symmetry were investigated. When the form of the low wavenumber energy spectrum was the Batchelor and Proudman k^4 type, it was determined by LES that the flow asymptotically approached isotropy on all scales. However, when the low wavenumber spectrum took the Saffman k^2 form, the largest scales of the flow remained anisotropic for all times, with the ratio of the mean-square velocity along the axis of symmetry over that perpendicular to the axis approaching 1.5 for impulsive forces directed along the symmetry axis, and 0.8 for impulsive forces directed perpendicular to the symmetry axis. Isotropic turbulence corresponds to a value of unity for this ratio. However, even though the energy-containing scales of motion remained anisotropic, the smallest scales of the flow approached isotropy, consistent with the concept of local isotropy of the small-scale turbulence discussed earlier. Use of an isotropic subgrid-scale model to represent these small scales was thus justified *a posteriori*. Note that the subgrid-scale model itself is incapable of isotropizing the small scales of the flow since an isotropic eddy viscosity transport coefficient can not transport energy from one velocity component to another. Rather, the approach to isotropy of the smallest scales of the large-eddy simulation was due to the resolved-scale pressure forces.

A remarkable feature of the simulation results for the decay of axisymmetric turbulence with a Saffman k^2 low wavenumber coefficient was the development of an asymptotic similarity state with the same power-law exponents of the isotropic turbulence decay despite the evident anisotropy of the energetic scales of motion. The existence of the same Saffman invariant and no other relevant dimensional quantities apparently forced the same similarity scaling on the axisymmetric turbulence decay as occurs for the isotropic turbulence decay.

In considering the decay of isotropic turbulence, Chasnov (1994) also intro-

duced a uniform mean passive scalar gradient across the flow and studied the generation of passive scalar fluctuations from the mean scalar gradient by turbulent motion along the direction of the gradient. Such a uniform gradient satisfies the requirement of statistical homogeneity, but not isotropy. The scalar fluctuations that are subsequently generated are necessarily axisymmetric in their two-point correlations in physical space. Using the isotropic eddy-viscosity and diffusivity subgrid-scale model discussed above, Chasnov (1994) demonstrated the establishment of a new asymptotic similarity state for this passive scalar field. Excellent agreement was found between the simulation results and a simple scaling argument based on the low wavenumber energy spectrum invariant. Furthermore, the results of this LES were in good qualitative agreement with earlier experimental grid-turbulence results of Sirivat and Warhaft (1983), but were of higher precision due to the length of the time integrations. Wind tunnels are simply not long enough to compete with the precision obtainable by LES.

Asymptotic similarity states of homogeneous turbulence with buoyancy forces have also been successfully simulated by LES. In the work of Batchelor *et al.* (1992), initially-isotropic density fluctuations are introduced in a fluid at rest, and subsequent (anisotropic) velocity fluctuations are generated by the buoyancy force. LES was used for two purposes in this work. First, a complete study of the maximum mean-square velocity generated by the initial density distribution as a function of an initial pseudo-Reynolds number of the flow was undertaken. This Reynolds number is constructed using a characteristic length scale of the initial density distribution and a characteristic magnitude of the initial buoyancy force. Direct numerical simulations were adaquate for relatively low Reynolds numbers but were unable to be extended into the regime where it was suspected that the maximum mean-square velocity became Reynolds-number independent. In fact, this Reynolds-number independence only occurs after the Reynolds number is sufficiently large that an inertial subrange begins to develop before the mean-square velocity reaches its maximum value; direct numerical simulations are presently incapable of reaching such large Reynolds numbers. The introduction of a k-dependent eddy viscosity provided the solution of this numerical difficulty. As the initial Reynolds number of the flow is increased, the molecular viscosity becomes less and less important with respect to the subgrid-scale eddy viscosity ($\nu << \nu_e$), and the maximum value attained by the mean-square velocity necessarily becomes Reynolds-number independent. However, there was in fact no guarantee that such a maximum value of the mean-square velocity existed, since it was not found by a linear analysis of the flow evolution (given some generic initial density fluctuations).

The long-time high Reynolds number asymptotic state of homogeneous buoyancy-generated turbulence was also studied. Large-eddy simulations demonstrated that the mean-square velocity, density variance and integral scales follow approximate power-laws in time asymptotically. Furthermore, the Reynolds number of the flow at time t, defined in the usual way, is an increasing function of time, providing this flow a rather unique character. These numerical results then motivated very simple and appealing dimensional arguments that predict all of the exponents discovered

numerically.

Further work on buoyancy-generated turbulence appears in a more recent publication (Chasnov 1995b). Here, the previous large-eddy simulations of buoyancy-generated turbulence were extended to include the transport of additional passive scalar fields by the turbulence. Accordingly, eddy viscosity and diffusivity subgrid-scale models were employed for each of the velocity, density and passive scalar fields. Asymptotic similarity states were computed by LES for the passive scalar fields with and without uniform mean scalar gradient, giving results in excellent agreement with corresponding generalizations of earlier dimensional arguments.

Finally, some continuing work involving the large-eddy simulations of rotating and stably-stratified homogeneous turbulence (Squires *et al.* 1994, Chasnov 1995c) should be briefly mentioned. These flows are distinguished from the ones discussed above in that an additional time scale enters the problem, namely the period of the internal wave motion, be it inertial waves for the rotating turbulence or gravity waves for the stably-stratified turbulence. Dimensional arguments to determine the asymptotic similarity states in these flows are accordingly incomplete in that a dimensionless ratio formed from the period of the internal waves to the turbulence time scale exists. This additional freedom also results in a very interesting phenomenon that has sometimes been referred to in the past as a "two-dimensionalization" of these flows. Namely, the vertical integral scale of the turbulence may behave asymptotically quite different than the horizontal integral scale. (Vertical here is defined as the direction either along the rotation axis or parallel to the gravitational force). Figure 7.14 presents results from large-eddy simulations for the time-evolution of the horizontal and vertical integral scales in rotating and stably-stratified decaying homogeneous turbulence. The integral scales are defined for the different velocity components in the rotating flow, and as an integral scale of the "energy" (kinetic and potential) in the stably-stratified flow. In the rotating flow, the vertical integral scale of the horizontal velocity correlation grows much faster than all other integral scales. This effect has also been observed in experiments (Jacquin *et al.* 1990). In the stably-stratified flow, the vertical integral scale apparently approaches a constant, whereas the horizontal integral scale increases indefinitely. These are very interesting effects and the asymptotic similarity states which are being developed in these flows are still under investigation.

7.6.2 Wall-bounded flows

The presence of a solid boundary affects the physics of the subgrid scales in several ways. First, the growth of the small scales is inhibited by the presence of the wall. Secondly, the exchange mechanisms between the resolved and unresolved scales are altered; finally, in the near-wall region the subgrid scales may contain some significant Reynolds-stress producing events, and the SGS model must account for them.

Consider, for instance, a turbulent "event" (for instance, an ejection of low-speed fluid from the near-wall layer) occurring near a solid boundary (the shaded

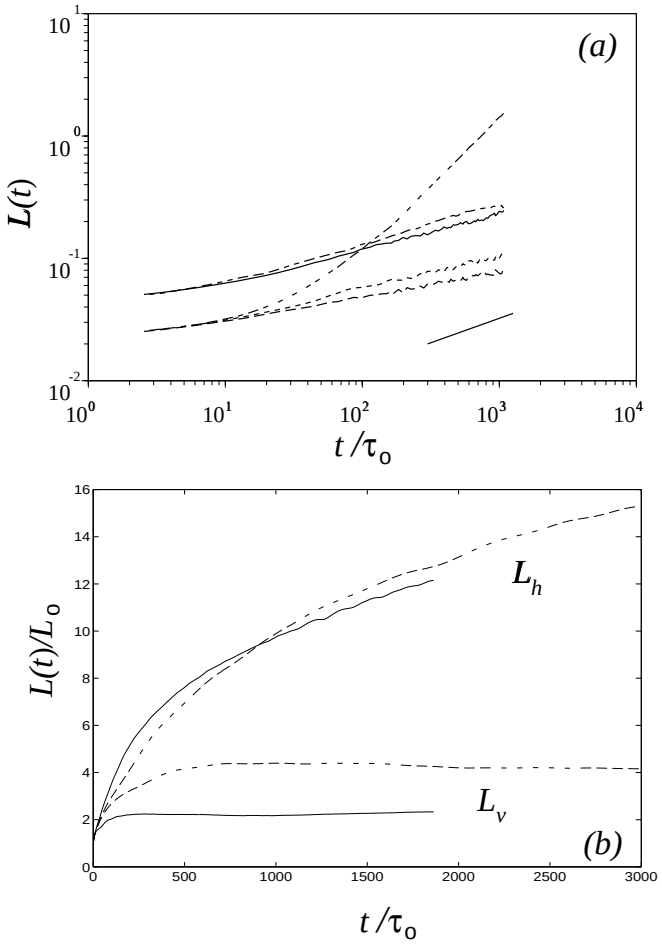

Figure 7.14: Time evolution of the horizontal and vertical integral scales in rotating and stably-stratified homogeneous turbulence. (a) Rotating turbulence. Plotted are the horizontal and vertical integral scales for the various velocity components and correlations. The rapidly growing integral scale corresponds to the vertical correlation of the horizontal velocity components. The lowest straight line is the theoretical result for isotropic turbulence (from Squires *et al.* 1994). (b) Stably-stratified turbulence. The solid and dashed lines correspond to simulations with different initial Froude numbers (from Chasnov 1995c).

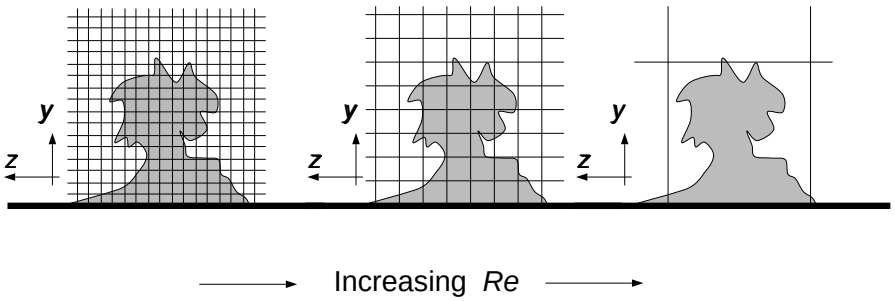

Figure 7.15: Grid resolution and near-wall structures.

area in Fig. 7.15); if the mesh is very fine, the effect of this event will appear exclusively through the resolved velocity. If the grid is coarsened or, equivalently, the Reynolds number increased for constant mesh spacing, part of the event becomes due to the unresolved scales, and the SGS model must account for part of the energy produced by it. If the mesh is coarsened further (or the Reynolds number increased), all the energy production may occur at the subgrid-scale level, and must be taken into account either through approximate boundary conditions, or through modifications to the eddy viscosity.

In simulations in which the wall layer is resolved, the most common way to account for these phenomena is by decresasing the length scale in the eddy viscosity. Moin *et al.* (1978) and Moin and Kim (1982), for example, used a two-part model similar to that introduced by Schumann (1975):

$$\tau_{ij} = -2\nu_T \left(\overline{S}_{ij} - \langle\overline{S}_{ij}\rangle\right) - 2\nu_T^*\langle\overline{S}_{ij}\rangle, \tag{7.64}$$

where $\langle\cdot\rangle$ represents averaging over planes parallel to the wall. The first term in (7.64) is a Smagorinsky term modified to eliminate the effect of the mean shear, and to model the SGS stresses as if the flow were isotropic:

$$\nu_T = \left\{C_s\Delta[1-\exp(-y^+/25)]\right\}^2 \left[2\left(\overline{S}_{ij} - \langle\overline{S}_{ij}\rangle\right)\left(\overline{S}_{ij} - \langle\overline{S}_{ij}\rangle\right)\right]^{1/2}, \tag{7.65}$$

(where $\Delta^3 = \Delta x\Delta y\Delta z$ and $C_s = 0.1$); the second term, in which

$$\nu_T^* = \left\{0.25\Delta z[1-\exp(-{y^+}^2/25^2)]\right\}^2 \left[2\langle\overline{S}_{ij}\rangle\langle\overline{S}_{ij}\rangle\right]^{1/2}, \tag{7.66}$$

is designed to account for the inhomogeneity due to the non-zero mean shear, and for the production of subgrid-scale energy in the near-wall region. Wall effects were included by the introduction of Van Driest (1956) damping to represent the reduced growth of the small scales near the wall.

Their results were in excellent agreement with experimental data. The wall-layer dynamics were also captured well; the low-speed streaks, for instance, had the correct length ($\lambda_x^+ \simeq 1,200$), although their spacing was high ($\lambda_z^+ \simeq 200$).

Piomelli *et al.* (1988) modified the Van Driest damping term to give the correct near-wall behavior for the SGS stress ($\tau_{12} \sim {y^+}^3$); they calculated the flow in a

plane channel at Reynolds numbers in the range $Re_\tau = 180 - 640$, and found that the choice of model must be coupled with that of the filter, and that an inconsistent choice gives inaccurate results. When the Gaussian filter is used and the Leonard stresses are computed, for instance, inclusion of the scale similar model (Bardina *et al.* 1983) gives more accurate results than the Smagorinsky part alone. When the Fourier cutoff filter is used, on the other hand, the scale-similar part of the model is identically zero, and the Smagorinsky model alone is consistent and gives satisfactory results. Mean velocity, turbulence intensities and velocity spectra were compared, and the agreement between filtered DNS data and LES results was very good. The mean streak spacing was also predicted accurately, although a coarser mesh was used than the one employed by Moin and Kim (1982).

One of the most useful characteristics of the dynamic eddy viscosity of Germano *et al.* (1991) is the fact that the correct near-wall behavior of the SGS stresses is ensured without the need for ad hoc adjustments or wall damping functions. This results in reduced SGS dissipation in the near-wall region compared with the Smagorinsky model, and more accurate prediction of the turbulence physics there.

Piomelli (1993b) used this model for the calculation of plane channel flow at Reynolds numbers in the range $Re_\tau = 200-2,000$. The results of these calculations were in very good agreement with DNS and experimental data. The rms turbulence intensities exhibited no loss of accuracy in the near-wall region even at the highest Reynolds number; the location and magnitude of the peak streamwise turbulence intensity were predicted correctly even in the low-resolution calculation. Higher moments, such as the skewness factor of the large-scale velocity, were also in good agreement with the data.

These calculations also evidenced how the resolution of the energy-producing events affects the SGS model. Contours of streamwise velocity fluctuation $u'' = \overline{u}_i - \langle \overline{u}_i \rangle$ in an xz-plane near the wall are shown in Fig. 7.16. The contours of u'' for the $Re_\tau = 200$ case resemble those obtained from direct simulations. As the mesh becomes coarser (in wall units), however, the structures tend to become wider and less elongated in the streamwise direction (an observation confirmed by the two-point correlations), as a result of the inadequate grid resolution at high Reynolds number. The two $Re_\tau = 1,050$ calculations highlight this difference: the contours of u'' are significantly more diffused, and fewer large Reynolds stress events are observed, when the coarse mesh is used; the less frequent occurrence of high-intensity v fluctuations is also responsible for decreased flatness of v in this region.

A comparison of the length scales used in the dynamic model, $\ell_d = (C\overline{\Delta}^2)^{1/2}$, and in the Smagorinsky model, $\ell_s = 0.1\overline{\Delta}[1 - \exp(-y^+/25)]$ is shown in Fig. 7.17. The length scale ℓ_s is almost ten times larger than ℓ_d in the near-wall region, resulting in a subgrid-scale dissipation that is one hundred times larger. Even if the damping function in the expression for ℓ_s is changed to account for the near-wall behavior of τ_{12} as recommended by Piomelli *et al.* (1988), where the length scale used is $\ell_p = 0.1\overline{\Delta}[1 - \exp(-{y^+}^3/25^3)]^{1/2}$, the Smagorinsky model remains more dissipative than the dynamic model.

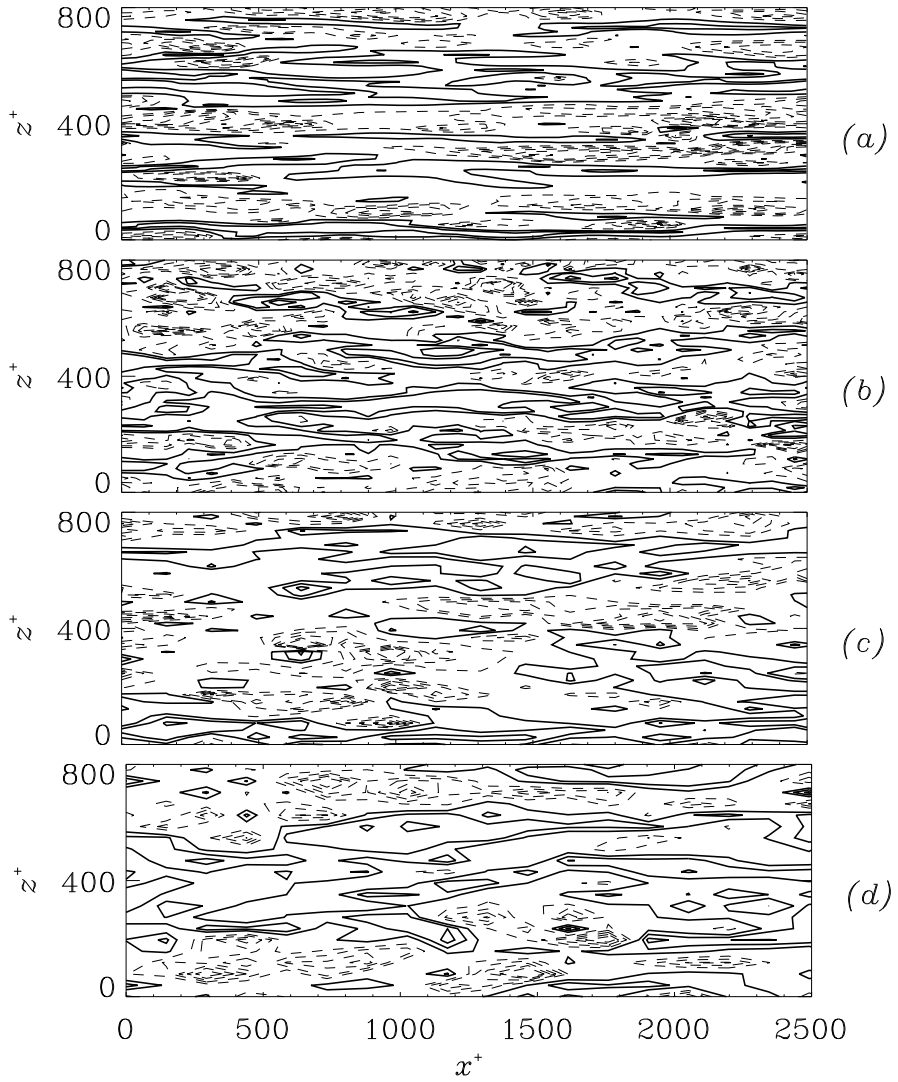

Figure 7.16: Contours of streamwise velocity fluctuations u'' in the $y^+ \simeq 6$ plane (from Piomelli 1993). Dashed lines indicate positive contours. (a) $Re_\tau = 200$; (b) $Re_\tau = 1,050$, fine mesh; (c) $Re_\tau = 1,050$, coarse mesh; (d) $Re_\tau = 2,000$.

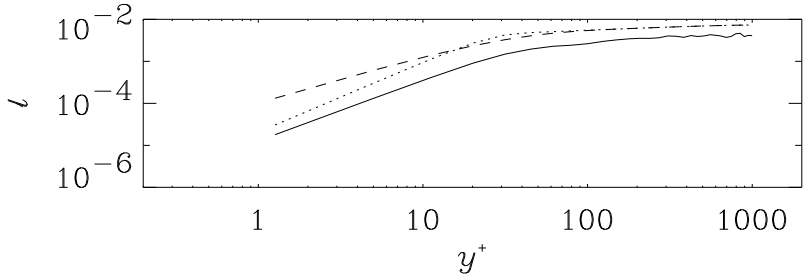

Figure 7.17: Comparison of dynamic model and Smagorinsky model length scales (from Piomelli 1993). —— ℓ_d (dynamic model); - - - ℓ_s (Smagorinsky model); ····· ℓ_p (Smagorinsky model with correct asymptotic behavior).

The reduced subgrid-scale dissipation is due to the occurrence of local backscatter. Near the wall the length scale remained essentially the same when the mesh was coarsened. This effect is counter-intuitive: one would expect that, as the grid becomes coarser, the length scale representative of the subgrid-scales increase. It can be explained by examining the model behavior in the near-wall region. Locally, the quantity $\mathcal{L}_{ij}M_{ij}$, which appears in the numerator of (7.52), can be of either sign; it is negative on the average, resulting in a positive coefficient C, reflecting the fact that the small scales are dissipative even in the near-wall region. The effect of localized regions where $\mathcal{L}_{ij}M_{ij} > 0$, however, is to reduce the value of the coefficient and, therefore, the length scale, thereby accounting for subgrid-scale backscatter, albeit only in an average sense. To illustrate this point, in Fig. 7.18 are shown the positive and negative contributions to C, defined as

$$C_f = -\frac{1}{4}\frac{\langle \mathcal{L}_{ij}M_{ij} - |\mathcal{L}_{ij}M_{ij}|\rangle}{\langle M_{mn}M_{mn}\rangle}, \qquad C_b = -\frac{1}{4}\frac{\langle \mathcal{L}_{ij}M_{ij} + |\mathcal{L}_{ij}M_{ij}|\rangle}{\langle M_{mn}M_{mn}\rangle}. \tag{7.67}$$

The forward- and backward-scatter contributions to the SGS dissipation, $\varepsilon_{sgs} = \tau_{ij}\overline{S}_{ij}$, are consequently given by

$$\varepsilon_f = -C_f\overline{\Delta}^2|\overline{S}|^3, \qquad \varepsilon_b = -C_b\overline{\Delta}^2|\overline{S}|^3. \tag{7.68}$$

It can be seen from Fig. 7.18a that there is a substantial negative contribution to C across the channel, due to the fact that $\mathcal{L}_{ij}M_{ij} > 0$ at nearly 50% of the points. This negative contribution is, effectively, a correction to the eddy viscosity, that is decreased due to local subgrid-scale backscatter. In the coarse-grid calculation, both positive and negative contributions to C in the near-wall region are substantially smaller than when the fine-grid is used, but the positive and negative contributions to the SGS dissipation are similar (Fig. 7.18b), and the net SGS dissipation (not shown) is essentially the same for both calculations. In the near-wall region the percentage of points where $\mathcal{L}_{ij}M_{ij} > 0$ increases; SGS backscatter occurs at the same locations where the energy production is large, but the average backscatter predicted by the model is not as high as expected based on the *a priori* results (Piomelli *et al.* 1991) probably due to the less frequent occurrence of strong $u''v''$ events.

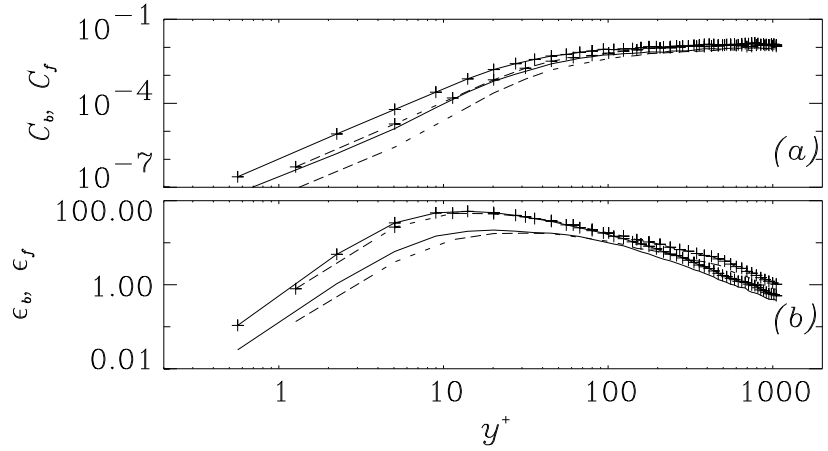

Figure 7.18: Backward and forward contributions to the model coefficient and to the subgrid scale dissipation. $Re_\tau = 1,050$ (from Piomelli 1993). (a) Model coefficient. —— $-C_b$, fine mesh; ····· $-C_b$, coarse mesh; +——+ C_f, fine mesh; +·····+ C_f, coarse mesh. (b) SGS dissipation. —— $-\epsilon_b$, fine mesh; ····· $-\epsilon_b$, coarse mesh; +——+ ϵ_f, fine mesh; +·····+ ϵ_f, coarse mesh.

Although adjustments to the eddy viscosity in the near-wall region can yield more accurate prediction of the turbulent statistics, the number of grid points required to resolve the near-wall region limits to the Reynolds number attainable by LES calculations in which the wall layer is resolved. The use of unstructured or block-structured meshes, in which the grid can be coarsened in *all* directions as one moves away from the wall (as opposed to grids that are stretched in one direction only as is commonly done) can alleviate this limitation, but not remove it altogether. Chapman (1979) estimated that the resolution required to resolve the outer layer of a growing boundary layer is proportional to $Re^{0.4}$, while for the viscous sublayer (which, in aeronautical applications, only accounts for approximately 1% of the boundary layer thickness) the number of points needed increases like $Re^{1.8}$.

One way to overcome this problem is to use approximate boundary conditions similar to the wall functions employed in Reynolds stress models. Approximate boundary conditions assume that the dynamics of the wall layer are universal, and that some generalized law-of-the-wall can be imposed. The approximate boundary conditions imposed so far have been quite simple, usually based on the existence of an equilibrium layer and a logarithmic velocity profile.

Deardorff (1970), in his channel flow computations, forced the existence of a logarithmic layer, and made the additional assumption that the turbulent fluctuations be isotropic:

$$\frac{\partial^2 \overline{u}}{\partial y^2} = -\frac{1}{\kappa(\Delta y/2)^2} + \frac{\partial^2 \overline{u}}{\partial z^2}, \tag{7.69}$$

$$\overline{v} = 0 \text{ at the wall,} \tag{7.70}$$

$$\frac{\partial^2 \overline{w}}{\partial y^2} = \frac{\partial^2 \overline{w}}{\partial x^2}. \tag{7.71}$$

In the same flow, Schumann (1975) used conditions that related the wall stress to the velocity in the core by

$$\tau_{12} = \frac{\langle \tau_w \rangle}{\langle \overline{u}(x, y_2, z) \rangle} \overline{u}(x, y_2, z) \tag{7.72}$$

$$\overline{v} = 0 \text{ at the wall} \tag{7.73}$$

$$\tau_{32} = \frac{1}{Re_\tau} \frac{\overline{w}(x, y_2, z)}{\Delta y/2}. \tag{7.74}$$

These equations, in which y_2 refers to the first grid point off the solid wall, impose that the wall stress is proportional to the velocity at the first point (both in the streamwise and spanwise directions). The mean stress $\langle \tau_w \rangle$ can be known for a given pressure gradient, or can be calculated iteratively by requiring that the plane-averaged velocity at the first grid point, $\langle \overline{u}(x, y_2, z) \rangle$, satisfy the logarithmic law (Grötzbach 1981).

Piomelli *et al.* (1989) applied conditions similar to (7.72–7.74); however, they required the wall stress to be correlated to the instantaneous velocity some distance downstream of the point where the wall stress is required, to take into account the inclination of the elongated structures in the near-wall region:

$$\tau_{12}(x, 0, z) = \frac{\langle \tau_w \rangle}{\langle \overline{u}(x, y_2, z) \rangle} \overline{u}(x + \Delta_s, y_2, z) \tag{7.75}$$

(and a similar one for τ_{32}) where Δ_s is a streamwise displacement; its optimum value can be obtained from DNS or experimental data and is approximately $\Delta_s = z_2 \cot 8^o$ for $30 < y_2^+ < 50$, and $\Delta_s = y_2 \cot 13^o$ for larger distances. The plane-averaged wall stress was obtained solving iteratively a generalized law-of-the-wall that is also valid for flows with transpiration.

Balaras *et al.* (1995) applied the shifted model (7.75) in conjunction with the dynamic SGS model to study the flow in a plane channel at high Reynolds number, with results in excellent agreement with experimental, DNS and resolved LES data. Fig. 7.19 shows the comparison of the root-mean-square streamwise fluctuations for two Reynolds numbers, $Re_\tau = 200$ and 5,000, with DNS and experimental data. It is interesting to notice that there is very little difference between the the Smagorinsky and dynamic model results, except at the first grid point. This is a reflection of the fact that the model coefficient was nearly constant throughout most of the channel, and its value ($C \simeq 0.02$) was close to that of the Smagorinsky constant for isotropic flows, $C_S^2 \simeq 0.03$ (Fig. 7.20). This indicates that perhaps in the core of the flow, and at high Reynolds numbers, the turbulent eddies obey inertial range dynamics. Under these conditions even a simple model such as the Smagorinsky model gives acceptable results. Only near the wall the physics of the small scales require more sophisticated modeling.

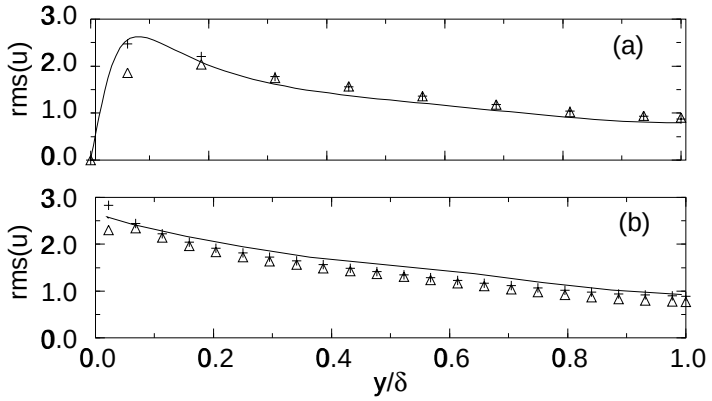

Figure 7.19: Plane-averaged streamwise turbulence intensity $\langle u''^2 \rangle^{1/2}$ (from Balaras *et al.* 1995). (a) $Re_\tau = 200$, + dynamic model, △ Smagorinsky model, —— DNS (Kim *et al.* 1987); (b) $Re_\tau = 5,000$, + dynamic model, △ Smagorinsky model, —— experiment (Comte-Bellot 1963).

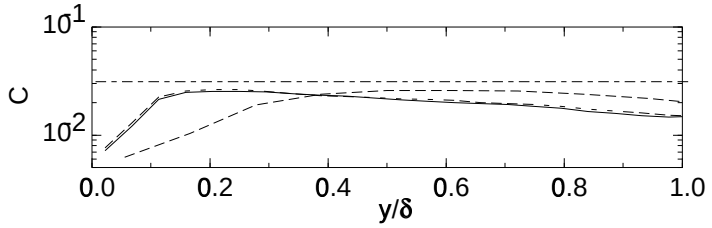

Figure 7.20: Model coefficient (from Balaras *et al.* 1995). ····· $Re_\tau = 400$, —— $Re_\tau = 1,000$, — — — $Re_\tau = 5,000$, —·— Smagorinsky coefficient C_S^2.

The models described above are all based on the use of generalized laws-of-the-wall; they require that the near-wall be nearly in equilibrium. If such is not the case, models of this type are bound to give incorrect answers. More general approximate boundary conditions are required to predict the flow in complex geometries (including strong acceleration, secondary mean velocity gradients, separation and reattachment, for instance) where the logarithmic layer may not exist.

7.6.3 Transitional and relaminarizing flows

Many flows of engineering interest, especially involving aeronautical applications, include regions of transitional or relaminarizing flow. In transitional regions various types of perturbations grow, interact with the mean flow and with each other. In engineering flows, this growth will frequently result in a turbulent regime.

Subgrid-scale models, which are usually based on high Reynolds number dynamics, often have difficulty in calculations of transitional or relaminarizing flows. The eddy viscosity predicted by the Smagorinsky model, for instance, is non-zero even in laminar flows. The additional dissipation introduced by the model in laminar flow is non-physical, and has the effect of damping excessively the growth of the small perturbations.

If the initial perturbations are large enough, even LES calculations that use the Smagorinsky model will eventually result in a turbulent flow. It is, however, very important, from a technological point of view, to predict the transition process correctly (*i.e.*, with the correct temporal or spatial development and properties), particularly since the peak skin friction and heat transfer usually occur toward the end of the transition process.

Piomelli and coworkers studied the fundamental transition in a flat-plate boundary layer (Piomelli *et al.* 1990a) and in a plane channel (Piomelli and Zang 1991), and found that when the Smagorinsky model is used, the linearly-unstable perturbations are damped. They introduced an *ad hoc* intermittency function that turned the SGS model off in laminar flow, and obtained good comparison of their results with theory and DNS.

The dynamic eddy viscosity model has the characteristic that the model coefficient vanishes in laminar flow, where $\mathcal{L}_{ij}$ is identically zero; this results in better prediction of the transition process without requiring the introduction of additional empirical information. Germano *et al.* (1991) computed the transitional and turbulent flow in a plane channel. They obtained very good agreement with the theory in the linear stages of the growth, where the model gave no contribution and the perturbations were completely resolved, and with the DNS data during the nonlinear stages of the breakdown, where the eddy viscosity increased to account for the broadening of the spectrum.

In Fig. 7.21 the time-development of the plane-averaged wall stress is shown. The dynamic model calculation gives better results than either the Smagorinsky model with the *ad hoc* intermittency function, or the model based on the Renormalization Group Theory of Yakhot and Orszag (1986). The overshoot in the skin friction, which is of great interest in engineering applications, was captured

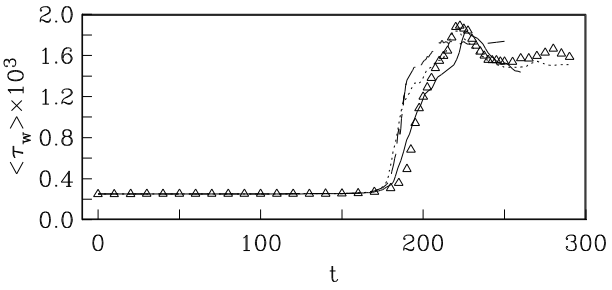

Figure 7.21: Time evolution of the wall stress (from Zang and Piomelli 1993). ····· Scaled Smagorinsky model (Piomelli and Zang 1991); – – – RNG model (Piomelli *et al.* 1990b); ——— dynamic eddy viscosity model (Germano *et al.* 1991); △ fine direct simulation (Zang *et al.* 1991).

accurately. The time-development of the principal Fourier modes was also in good agreement with the DNS data throughout the nonlinear stages. The streamwise turbulent intensities (Fig. 7.22) were also in better agreement with the DNS data than those obtained with the other models.

An additional difficulty in transitional flows is that, during the nonlinear interaction stages of the breakdown, very small structures (thin shear layers, for instance) are generated, that must be resolved even in an LES. In the calculations of fundamental breakdown by Germano *et al.* (1991), for instance, the mesh was refined as the calculation progressed, and it was found that the finest grids (and smallest time step) were required not in the turbulent region, but during the nonlinear stages ($t \simeq 200$). A similar problem occurs if regions of the flow are inviscidly unstable: Akselvoll *et al.* (1995), for instance, in their calculation of the flow in a backward-facing step, found that a very fine grid was required to resolve the instability of the shear layer emanating from the step.

An important question, especially for the simulation of transitional flows, regards the capability of the LES to resolve the large vortical structures that arise during the transition process. Given that the resolution of an LES calculation is, by definition, marginal (in the sense that the smallest resolved structures still contain a substantial amount of energy) one should expect that the Λ-vortices, shear layers *etc.* will not be as sharp and well resolved as they are in DNS calculations. Fig. 7.23 shows the vertical shear $\partial u/\partial y$ in an xy-plane from the simulation of subharmonic transition in a flat-plate boundary layer. The Reynolds number at the inlet is $Re = U_\infty \delta^*_{in}/\nu = 600$, which increases to 805 in the turbulent region ($x \simeq 800$), to match the experiment of Kachanov and Levchenko (1984). One can observe very clearly the development of a shear layer (on the left in the picture) that is lifted from the wall and develops the kinks characteristic of the multiple-spike stages. Initially, the shear layer is very well resolved; at later times, however, as it is convected downstream and the instability grows, one observes some oscillations in the lower-level contours, indicative of marginal resolution. The eddy

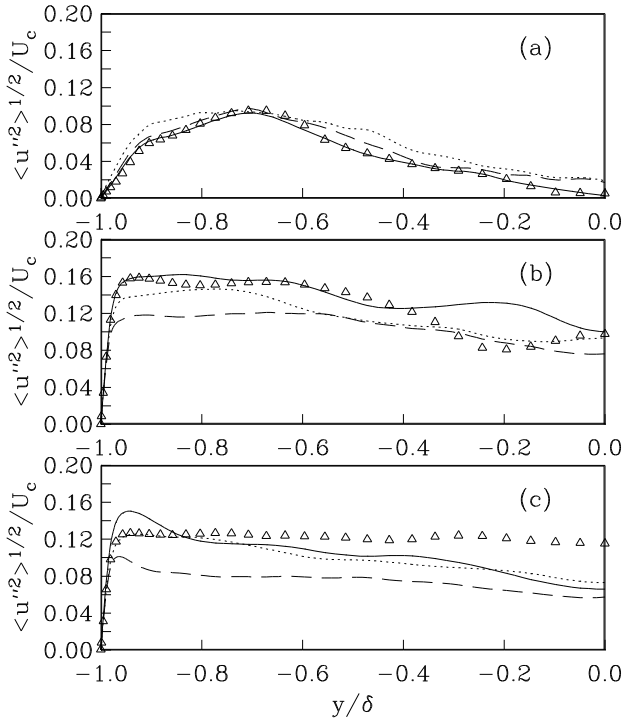

Figure 7.22: Plane-averaged streamwise turbulence intensity $\langle u''^2 \rangle^{1/2}$ (from Zang and Piomelli 1993). ····· Scaled Smagorinsky model (Piomelli and Zang 1991); - - - RNG model (Piomelli *et al.* 1990b); —— dynamic eddy viscosity model (Germano *et al.* 1991); △ fine direct simulation (Zang *et al.* 1991). (a) $t = 175$; (b) $t = 200$; (c) $t = 220$.

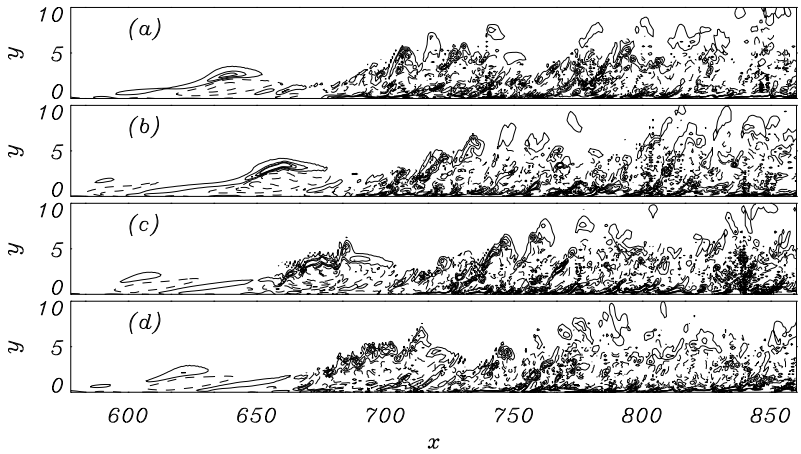

Figure 7.23: Vertical shear $\partial u/\partial y$ in the $z = 0$ plane. Subharmonic transition in a flat-plate boundary layer. (a) t_o; (b) $t_o + T/4$; (c) $t_o + T/2$; (d) $t_o + 3T/4$. T is the period of the fundamental wave.

viscosity (Fig. 7.24) is essentially zero in the laminar region, begins to rise at $x \simeq 700$, and becomes significant in a region in which the resolution is marginal. In the regions between the shear layers, the eddy viscosity is quite small, whereas sharp peaks can be observed where the shear layers are stronger and small scales are being generated. The added dissipation provided by the SGS model results in better resolution of the structures downstream of the points where the flow begins to break down. In general, even if the resolution is much coarser than in DNS (only $561\times65\times32$ grid points were used for the domain in the figure), the development of the transitional structures is predicted as well as the statistical quantities shown before. In the turbulent region, the eddy viscosity settles to values somewhat lower than in the laminar breakdown zone.

Situations in which the perturbations decay leading to a laminar or quasi-laminar state, also occur in engineering applications; relaminarization can take place in flows in which the Reynolds number decreases (for instance, in a duct that is being gradually enlarged) leading to an increase in the viscous dissipation, in highly accelerated flows in which the pressure forces dominate the Reynolds stresses, or in stably stratified and rotating flows (see Narasimha and Sreenivasan 1979).

The interaction of rotation and mean shear normal to the axis of rotation may also have either a stabilizing or a destabilizing effect on turbulence, depending on whether the angular velocity and mean shear have the same or opposite signs. In turbulent channel flow, for example, system rotation acts to both stabilize and destabilize the flow. On the unstable side Coriolis forces resulting from system rotation enhance turbulence-producing events, leading to an increase in turbulence levels, while on the stable side Coriolis forces inhibit turbulence production and decrease turbulence levels. The increase in the component energies, however, is

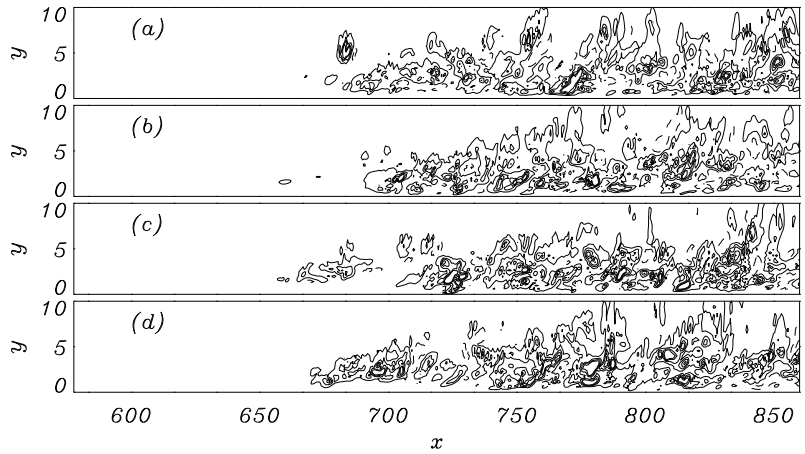

Figure 7.24: Eddy viscosity in the $z = 0$ plane. Subharmonic transition in a flat-plate boundary layer. (a) t_o; (b) $t_o + T/4$; (c) $t_o + T/2$; (d) $t_o + 3T/4$. T is the period of the fundamental wave.

dependent on the rotation rate: at sufficiently high rotation rates streamwise fluctuations on the unstable channel wall are suppressed relative to the non-rotating case. The stabilizing/destabilizing effects of rotation on turbulence in channel flow make this problem particularly challenging, since the SGS model is required to capture relaminarization with inactive turbulent motions as well as fully-developed turbulence.

Piomelli and Liu (1995) applied a localized dynamic model to the study of rotating channel flow for rotation rates in the range $Ro_b = \Omega(2\delta)/U_b = 0$ through 0.21 (where Ω is the angular velocity and U_b the bulk velocity) and Reynolds numbers $Re_b = U_b\delta/\nu$ between 5,700 and 23,000. They found that the localized SGS model gives better prediction of the turbulent fluctuations than the plane-averaged model, especially on the stable side of the channel (Fig. 7.25).

Full relaminarization on the stable side was observed in experiments (Johnston *et al.* 1972) and in the LES calculations of Tafti and Vanka (1992); in the DNS calculations of Kristoffersen and Andersen (1993) and in the DNS and LES computations of Piomelli and Liu (1995), however, the fluctuations on the stable side remained significant, and the mean velocity never reached the laminar profile, even at large rotation rates and at a Reynolds number at which relaminarization is expected to occur. The friction velocity u_τ normalized by the friction velocity in the absence of rotation $u_{\tau o}$, is plotted in Fig. 7.26. The LES, DNS and experimental data are in good agreement on the unstable side; in the experiment the bulk velocity was obtained from the volume flow rate, which led to underestimation of the bulk velocity (and an overestimation of Ro_b) because of the presence of boundary layers on the sides of the channel (see also Kristoffersen and Andersen 1993). The difference on the stable side, where the numerical results tend to lie close to the extrapolation of the results of experiments in which the flow remained turbulent

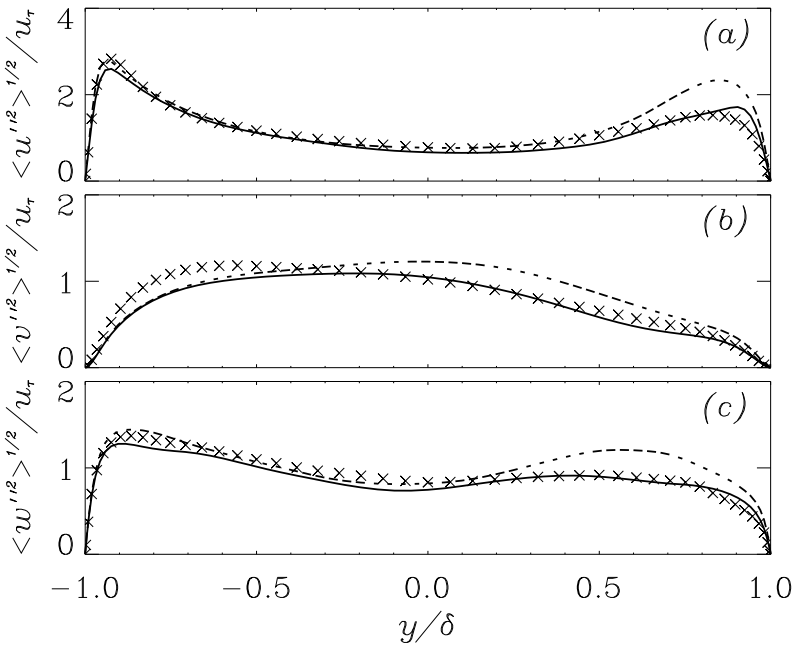

Figure 7.25: Turbulence intensities in the rotating channel. $Re_b = 5,700$, $Ro_b = 0.144$ (from Piomelli and Liu 1995). ——— Localized dynamic model; ····· plane-averaged dynamic model; × DNS. (a) u; (b) v; (c) w.

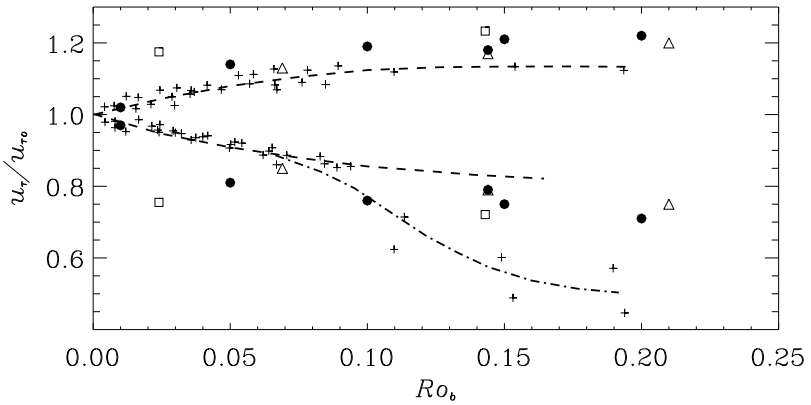

Figure 7.26: Friction velocity on the two sides of the channel (from Piomelli and Liu 1995). + Experiments, Johnston *et al.* (1972); • DNS; ▫ LES, Smagorinsky model, Tafti and Vanka (1992); △ LES, localized dynamic model, $Re_b = 5,700$. The lines are correlations of experimental data from Johnston *et al.* (1972).

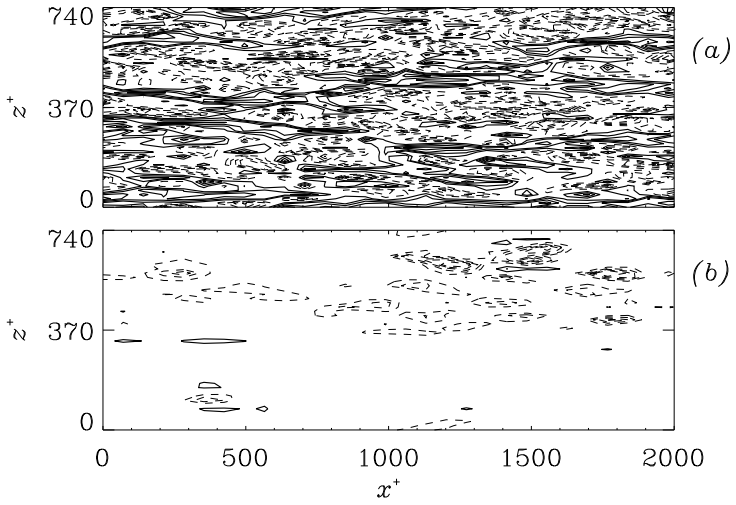

Figure 7.27: Streamwise velocity fluctuation contours in the xz-plane. $Re_b = 5,700$, $Ro_b = 0.210$, $y^+ = 5.4$. (a) Unstable wall; (b) stable wall. Contour lines are at intervals of ± 1; dashed lines indicate positive contours.

on the stable side (the dashed line), may be due to the relatively small aspect ratio of the experimental apparatus and the fact that the flow was not fully developed, which may have added a streamwise pressure gradient that could have increased the tendency of the flow towards relaminarization. The results obtained with the dynamic model are in much better agreement with the DNS results than those obtained by Tafti and Vanka (1992) with the Smagorinsky model, which tended to overdamp the fluctuations on the stable side, leading to excessively low wall stress even at the lower rotation rate they examined.

At the high rotation rates, longitudinal roll cells are formed that convect high momentum fluid in the downwash region between them. Figures 7.27 show contours of the u'' velocity fluctuations in two xz-planes near the unstable and stable walls near a local minimum and maximum of u_τ. The downwash of the roll cells appears as an elongated region of increased u'' velocity fluctuations at $z^+ \simeq 500$ To illustrate the response of the localized model to this phenomenon, contours of the model coefficient C are shown in Fig. 7.28, at the same time and locations as in the previous figure. The coefficient varies very significantly over the plane; on the stable side, larger values of C are observed where the velocity fluctuations are also large (i.e., in the downwash region of the roll cells); regions of backscatter (indicated by solid lines) can be observed.

7.6.4 Separated or highly three-dimensional flows

It was mentioned before that large-eddy simulations are based on the assumptions that the small scales are more isotropic, and less affected by the boundary

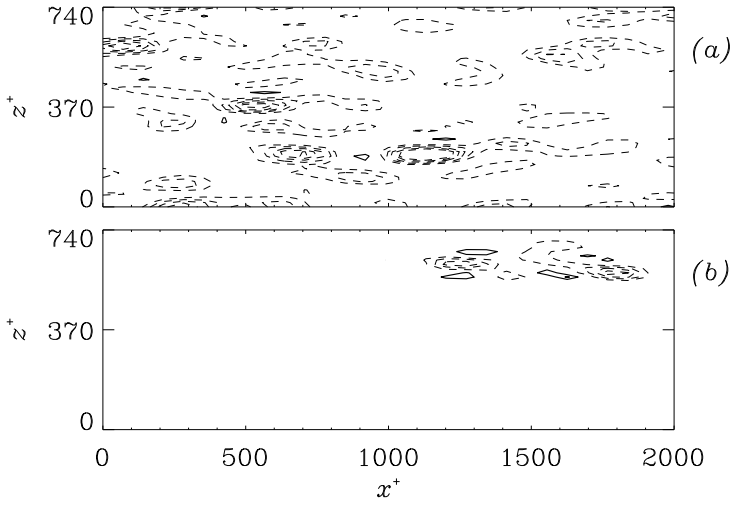

Figure 7.28: Model coefficient contours in the xz-plane. $Re_b = 5,700$, $Ro_b = 0.210$, $y^+ = 5.4$. (a) Unstable wall; (b) stable wall. Contour lines are at intervals of $\pm 5 \times 10^{-4}$; dashed lines indicate positive contours.

conditions, than the large scales. This assumption justifies the use of simple, equilibrium-based models, even in flows in which the resolved scales are clearly not in equilibrium. By the same token, LES should be more suitable than the Reynolds-averaged approach to study highly three-dimensional or separated flows, especially flows in which the gradient transport hypothesis, and hence one- and two-equation models of turbulence, fails. The application of secondary mean shear (in addition to the primary component $\partial U/\partial y$), for instance, has several important effects on the large scales, such as a reduction of the structure parameter, and also a difference between the angles formed by the velocity vector, the viscous shear stress vector, and the Reynolds shear stress vector. It is as yet unknown how significant the effects of mean flow three-dimensionality on the subgrid-scales are; present evidence, however, seems to indicate that, as long as the large scales are computed accurately, the application of the gradient-transport assumption to the small scales does not generate serious errors.

Liu (1994) and Liu *et al.* (1995) computed the flow in a turbulent boundary layer on which a pair of strong counter-rotating vortices was superimposed. They used a localized dynamic model. The vortices generate the extra strain components $\partial V/\partial y$, $\partial V/\partial z$, $\partial W/\partial y$ and $\partial W/\partial z$. The mean streamwise vorticity development, shown in Fig. 7.29, is predicted much more accurately than when $K - \varepsilon$ models are used, due to the fact that two-equation models cannot predict the gradients of the normal stress anisotropy, which play an important role in the devlopment of Ω_x.

Near the wall, under the principal vortices, secondary vorticity of the opposite sign is generated and lifted by the primary vortices. As the small-scale near-wall structures are convected towards the outer layer, they lose energy to the larger,

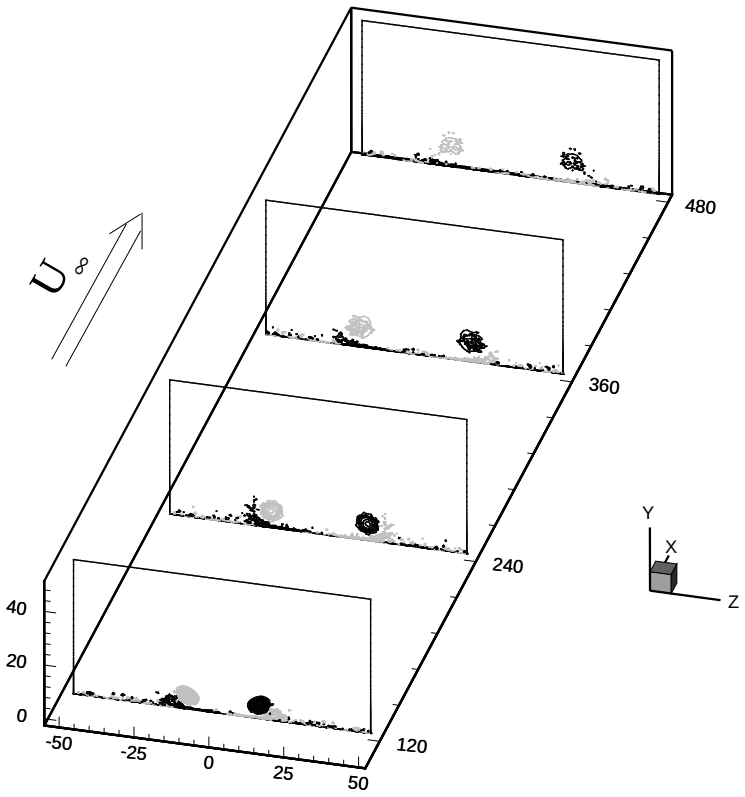

Figure 7.29: Vortex/boundary layer interaction. Contours of the mean streamwise vorticity Ω_x. Grey contours indicate positive vorticity.

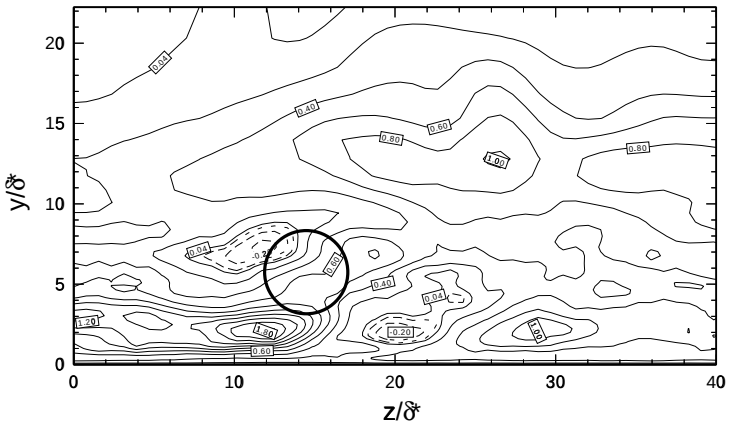

Figure 7.30: Vortex/boundary layer interaction. Contours of eddy viscosity ratio ν_T/ν at the second streamwise station. The black circle indicates the approximate location of the vortex core. $z = 0$ is the plane of symmetry.

outer-layer, structures; as a result, the SGS model predicts a region of negative eddy viscosity immediately outboard ($z/\delta^* = 20$) of the vortex core. Between the vortices, where the convection due to the common-flow-down pair results in thinning of the boundary layer, the eddy viscosity is large, and is maximum immediately inboard of the vortex, where the presence of a stagnation line creates a region of very strain rate, immediately inboard of which ($z/\delta^* = 8$) a saddle point is observed, with lower strain and eddy viscosity.

Akselvoll and Moin (1995) used several SGS models (the Smagorinsky model, the dynamic model and the dynamic localization model) in the computation of the flow behind a backward-facing step. All the models examined gave very good, and nearly identical, results. The mean velocity profiles downstream of the step, for instance, are shown in Fig. 7.31. Very good agreement is observed with the experiments; the reversed flow in the separted region is predicted very well, as is the reattachment point location. The eddy viscosity downstream of the step is shown in Fig. 7.32. The three models predict eddy viscosities that are significantly different (the dynamic localization model gives an eddy viscosity that, in the separated and reattachment regions is two to three times larger than the other models); the SGS dissipation predicted by the Smagorinsky and dynamic localization models, however, is essentially the same, less than twice that predicted with the dynamic model. The subgrid scales account for most of the energy dissipation, ε_{sgs} being generally three to seven times larger than the molecular dissipation.

Beaudan and Moin (1994) used the dynamic and Smagorinsky SGS models for the LES of the wake of a circular cylinder at $Re = 3,900$ (based on cylinder diameter and freestream velocity). The dynamic model gave results in better agreement with the experiments than the Smagorinsky model, especially in the

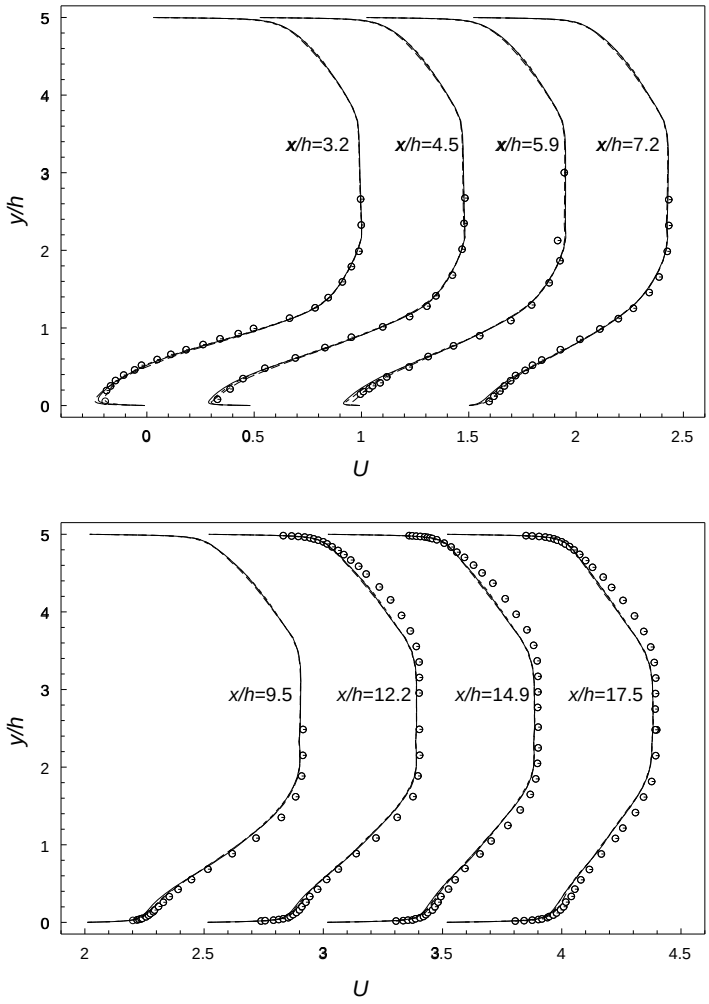

Figure 7.31: Mean velocity profiles downstream of a backward facing step (from Akselvoll and Moin 1995). ——— Dynamic model; – – – dynamic localization model; ····· Smagorinsky model; ∘ experiment (Adams *et al.* 1984).

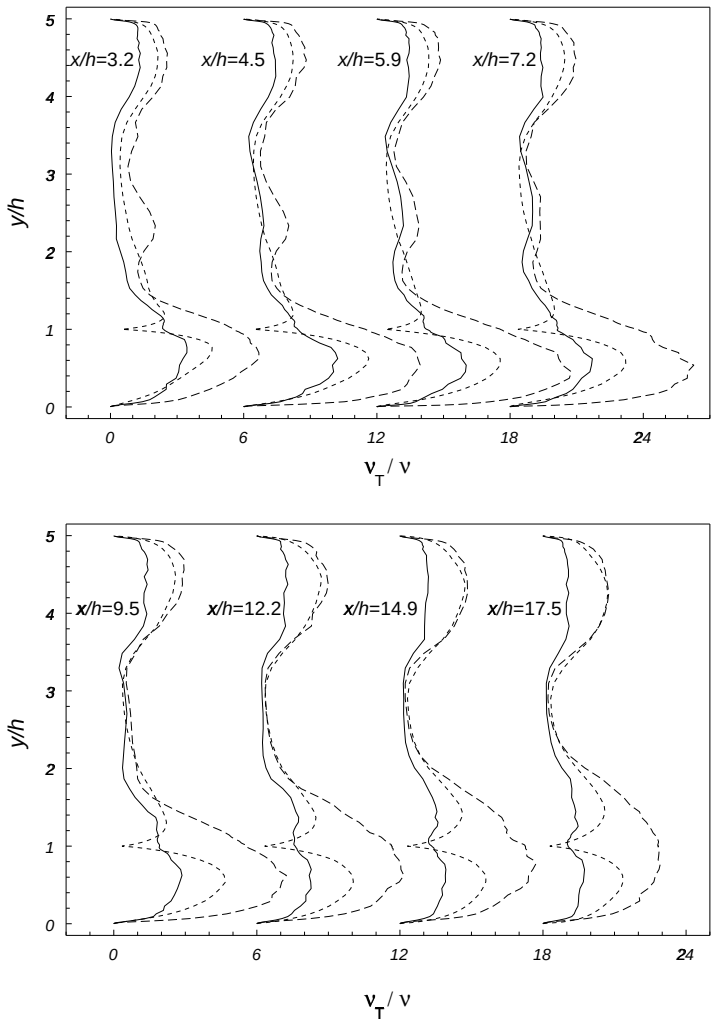

Figure 7.32: Eddy viscosity profiles downstream of a backward facing step (from Akselvoll and Moin 1995). $Re = 28,000$. ——— Dynamic model; – – – dynamic localization model; ····· Smagorinsky model.

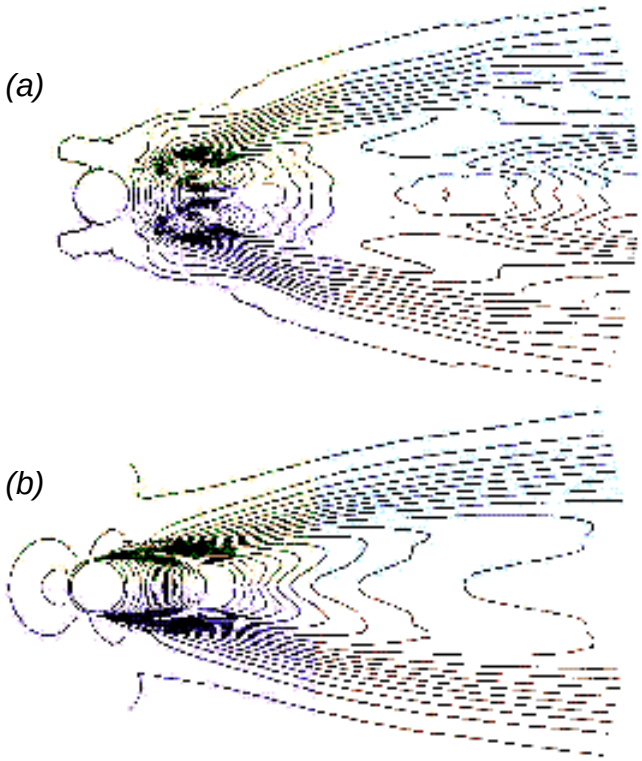

Figure 7.33: Eddy viscosity contours (normalized by the maximum ν_T) in the wake of a circular cylinder (from Beaudan and Moin 1994). (a) Dynamic model; (b) Smagorinsky model.

recirculation region behind the cylinder. The length of the separation bubble was predicted to within 2% of the experimental value when the dynamic model was used, while it was over-predicted by 29% with the Smagorinsky model (and by 17% if no model was used). Contours of the eddy viscosity for the two models are shown in Fig. 7.33. At this Reynolds number, the free shear layers are laminar; one whould, therefore, expect the eddy viscosity to be zero along them. The dynamic model predicts this behavior correctly, while the Smagorinsky model gives significant eddy viscosity in the shear layers all the way to the separation point on the cylinder.

7.7 Conclusions

In the hierarchy of methods for the solution of fluid flow problems, LES occupies an intermediate position between DNS and solution of the Reynolds-averaged Navier-Stokes equations (RANS). It will be successful as an engineering tool if its advantages over other techniques are exploited rather than if it is used to replace

either DNS or RANS modeling.

The principal advantage of LES over DNS is the fact that it allows one to compute flows at Reynolds numbers much higher than those feasible in DNS, or at the same Reynolds numbers but at a considerably smaller expense. One should not expect to be able to extract from LES the same information that can be extracted from DNS, since modeling the small scales affects high-order statistics more than the lower-order ones. Thus, LES is expected to be more reliable for first and second moments, and to reproduce qualitatively the basic structures of the flows (existence of shear layers, vortical structures and so on).

Large-eddy simulation is considerably more expensive than RANS techniques for flows that are one- or two-dimensional in the mean and steady. For this reason, it should be applied to problems in which its cost is comparable to that of the solution of the RANS equations or to problems in which lower-level turbulence models fail. Such problems include unsteady or three-dimensional boundary layers, vortex–boundary layer interactions, separated flows and flows involving geometries with sharp corners (in square ducts, for example). Although in the near future LES will still be limited to fairly simple geometries, significantly more complex flows should be studied than those examined so far. Large eddy simulation of these flows can also be used to provide data for the development of more accurate lower-level models (especially pressure statistics, which are difficult to measure experimentally).

So far, several turbulent and transitional "building block" flows have been studied by LES: homogeneous turbulence, shear flows, channel flow and boundary layers. Two types of calculations have been performed: high Re, unbounded flows or wall-bounded flows with approximate boundary conditions, or low to moderate Re flows, with fairly good resolution. Well-resolved calculations yield velocity fields that can be used to obtain information on turbulence structure, and that can provide information for lower-level models (Bardina *et al.* 1983; Moin and Kim 1985; Kim and Moin 1986). Presently, three-dimensional or non-equilibrium flows are being studied (such as the backward-facing step, vortex/boundary layer interactions, or three-dimensional boundary layers).

Large-eddy simulation research in engineering continues in many areas, with a particular focus on the following: the continued effort to devise more accurate models, especially for the near-wall region, the application to "complex flows", and, finally, the application of LES to compressible and reacting flows. The first issue is particularly important because of the need to extend LES to high Reynolds number flows, in which resolution of even the large structures in the near-wall region becomes unaffordable.

The application of LES to non-equilibrium flows is also a subject of great technological importance. For the time being, although the geometry constraints are being gradually removed as finite difference schemes supplant the spectral methods widely in use until now, the application of LES to engineering calculations in very complex geometries is not yet feasible. It may be perhaps more beneficial instead to use LES for detailed studies of the turbulence physics at moderate Reynolds numbers in non-canonical flows, to understand the basic phenomena at

play in new flow configurations, and to provide data for RANS models. Typical problems that are within the present capabilities of LES are flows that are three-dimensional in the mean, in fairly simple geometries, but that include one or more phenomena (extra strains, separation, pressure gradients, for example) that occur in more complex engineering flows.

Although the first applications of LES to compressible and reacting flows were relatively recent, much progress has already been made in this area. All of the most popular models have been extended to compressible flows, and a number of test cases have been examined. While many of the concerns that apply to incompressible applications (model accuracy, backscatter and so on) extend also to compressible flows, additional difficulties are due to the fact that the equations are more complex and shock wave interactions and eddy shocklets may occur; furthermore, finite differences introduce artificial dissipation, the effect of which must be studied and compared with that of the SGS dissipation. Aliasing errors can also be more significant, owing to the presence of triple products in the equations of motion. The simulation and modeling of flows including chemical reactions is still in its infancy.

Although large eddy simulations in engineering have not enjoyed a rapid development similar to that of direct simulations, the renewed activity in LES justifies an optimistic view of the future of this technique. One would hope that, ten years from today, LES of engineering problems will be routinely performed on a desktop workstation. To achieve this end a continued effort is required by the research community, involving increased interactions among its members. Experiments, direct simulations and numerical analysis are all necessary for further progress. The interaction between geophysical scientists and engineers, which has not been particularly noteworthy so far, must also be enhanced to facilitate the development of LES into a practical tool useful in both fields.

7.8 Acknowledgments

Ugo Piomelli acknowledges the support of the Office of Naval Research and of the NASA Langley Research Center. Jeff Chasnov wishes to thank R. Rogallo and A. Wray for the use of their software. The support of the Hong Kong Research Grant Council is also gratefully acknowledged.

7.9 References

Adams, E.W., Johnston, J.P., and Eaton, J.K. 1984 *Report No. MD-43*, Dept. Mech. Eng., Stanford University, Stanford, CA 94305.

Akselvoll, K., and Moin, P. 1995 *Report No. TF-63*, Dept. Mech. Eng., Stanford University, Stanford, CA 94305.

BALARAS, E., BENOCCI,C., AND PIOMELLI, U. 1995 *Theoret. Comput. Fluid Dynamics* **7**, 207.

BARDINA, J., FERZIGER, J.H., AND REYNOLDS, W.C. 1980 *AIAA Paper No. 80–1357.*

BARDINA, J., FERZIGER, J.H., AND REYNOLDS, W.C. 1983 *Department of Mechanical Engineering Report TF–19*, Stanford, California.

BARDINA, J., FERZIGER, J.H., AND ROGALLO, R.S. 1985 *J. Fluid Mech.* **154**, 321.

BATCHELOR, G.K. 1953 *The Theory of Homogeneous Turbulence*, (Cambridge University Press, Cambridge).

BATCHELOR, G.K. AND PROUDMAN, I. 1956 *Philos. Trans. R. Soc. London*, 248, 369.

BATCHELOR, G.K., CANUTO, V.M. AND CHASNOV, J.R. 1992 *J. Fluid Mech.* **235**, 349.

BEAUDAN, P., AND MOIN, P. 1994 *Report No. TF-62*, Dept. Mech. Eng., Stanford University, Stanford, CA 94305.

BERTOGLIO, J.P. 1985 In *Macroscopic modelling of turbulent flows*, ed. by U. Frisch, J.B. Keller, G. Papanicolaou, and O. Pironneau, (Springer-Verlag, Heidelberg), 100.

CABOT, W.H. AND MOIN, P. 1993 In *Large Eddy Simulation of Complex Engineering and Geophysical Flows*, ed. by B. Galperin and S.A. Orszag, (Cambridge University Press, Cambridge) 141.

CAMBON, C., JEANDEL, D. AND MATHIEU, J. 1981 *J. Fluid Mech.* **104**, 247.

CAMBON, C., JEANDEL, D. AND MATHIEU, J. 1989 *J. Fluid Mech.* **202**, 295.

CARATI, D., GHOSAL, S., AND MOIN, P. 1995 *Phys. Fluids* **7**, 606.

CHAPMAN, D.R. 1979 *AIAA J.* **17**, 1293.

CHASNOV, J.R. 1991a *Phys. Fluids A* **3**, 188.

CHASNOV, J.R. 1991b *Phys. Fluids A* **5**, 1164.

CHASNOV, J.R. 1993 *Phys. Fluids A* **5**, 2579.

CHASNOV, J.R. 1994 *Phys. Fluids***6**, 1036.

CHASNOV, J.R. 1995a *Phys. Fluids***7**, 600.

CHASNOV, J.R. 1995b *Phys. Fluids*, in press.

CHASNOV, J.R. 1995c *Dyn. of Atmos. and Oceans*, in press.

CHOLLET, J.P. AND LESIEUR, M. 1981 *J. Atmo. Sci.* **38**, 2747.

CHOLLET, J.P. 1984 In *Turbulent Shears Flow IV*, edited by F. Durst and B. Launder, (Springer-Verlag, Heidelberg), 62.

Clark, R.A, Ferziger, J.H. and Reynolds, W.C. 1979 *J. Fluid Mech.* **91**, 1.

Deardorff, J.W. 1970 *J. Fluid Mech.* **41**, 453.

Domaradzki, J.A, Metcalfe, R.W., Rogallo, R.S. and Riley, J.J. 1987 *Phys. Rev. Lett.* **58**, 547.

Germano, M. 1986 *Phys. Fluids* **29**, 2323.

Germano, M. 1992 *J. Fluid Mech.* **238**, 235.

Germano, M., Piomelli, U., Moin, P., and Cabot, W.H. 1991 *Phys. Fluids A* **3**, 1760.

Ghosal, S., and Moin, P. 1995 *J. Comput. Phys.* **118**, 24.

Ghosal, S., Lund, T.S., Moin, P., and Akselvoll, K. 1995 *J. Fluid Mech.* **286**, 229.

Grötzbach, G. 1981 *Int. J. Heat Mass Transfer* **24**, 475.

Herring, J.R. 1990 *Phys. Fluids A* **2**, 979.

Jacquin, L., Leuchter, O., Cambon, C. and Mathieu, J. 1990 *J. Fluid Mech.* **220**, 1.

Johnston, J.P., Halleen, R.M., and Lezius, D.K. 1972 *J. Fluid Mech.* **56**, 533.

Kachanov Y. S. and Levchenko V. Y. 1984 *J. Fluid Mech.* **138** 209.

Karniadakis, G.E. and Orszag, S.A. 1993 *Physics Today*, March, 34.

Kim, J. and Moin, P. 1986 *J. Fluid Mech.* **162**, 339.

Kolmogorov, A.N. 1941 *Dokl. Akad. Nauk. SSSR* **31**, 538.

Kraichnan, R.H. 1970 *J. Fluid Mech.* **70**, 189.

Kraichnan, R.H. 1976 *J. Atmos. Sci.* **33**, 1521.

Kristoffersen, R. and Andersson, H.I. 1993 *J. Fluid Mech.* **256**, 163.

Landau, L.D. and Lifshitz, E.M. 1959 *Fluid Mechanics*, Addison-Wesley.

Larcheveque, M. Chollet, J.P., Herring, J.R., Lesieur, M., Newman, G.R. and Schertzer, D. 1980 In *Turbulence Shear Flows II*, edited by Bradbury, J.S., Durst, F. Launder, B.E., Schmidt, F.W. and Whitelaw, J.H., (Springer-Verlag, Heidelberg), 50.

Leith, C.E. 1971 *J. Atmos. Sci.* **28**, 145.

Leith, C.E. 1990 *Phys. Fluids A* **2**, 297.

Leith, C.E. and Kraichnan, R.H. 1972 *J. Atmos. Sci.* **29**, 1041.

Leonard, A. 1974 *Adv. Geophys.* **18A**, 237.

LESIEUR, M. AND SCHERTZER, D. 1980 *J. Mec.* **17**, 609.

LESIEUR, M. 1990 *Turbulence in fluids* (Kluwer, Dordrecht).

LESIEUR, M. AND ROGALLO, R. 1989 *Phys. Fluids A* **1**, 718.

LESLIE, D.C. AND QUARINI, G.L. 1979 *J. Fluid Mech.* **91**, 65.

LILLY, D.K. 1967 In *Proc. IBM Sci. Comp. Symp. on Environmental Sciences*, Yorktown Heights, NY.

LILLY, D.K. 1992 *Phys. Fluids A* **4**, 633.

LIU, J. 1994 *Ph.D. Dissertation*, Dept. of Mech. Eng., University of Maryland–College Park.

LIU, J., PIOMELLI, U., AND SPALART, P.R. 1995 In *Turbulence 94: Theory and experiments*, edited by R. Benzi, (Kluwer, Dordrecht).

LOITSIANSKII, L.G. 1939 *Trudy Tsentr. Aero. Giedrodin. Inst.* **440**, 31.

LORENZ, E.N. 1969 *Tellus* **21**, 289.

LUND, T.S., GHOSAL, S. AND MOIN, P. 1993 In *Engineering Applications of Large Eddy Simulations*, edited by Ragab, S.A. and Piomelli, U., ASME, 7.

MASON, P. AND THOMSON, D. 1992 *J. Fluid Mech.* **242**, 51.

METAIS, O. AND LESIEUR, M. 1986 *J. Atmos. Sci.* **43**, 857.

METAIS, O. AND LESIEUR, M. 1992 *J. Fluid Mech.* **235**, 157.

MOIN, P., REYNOLDS, W.C., AND FERZIGER, J.H. 1978 *Department of Mechanical Engineering Report TF–12*, Stanford, California.

MOIN, P. AND KIM, J. 1982 *J. Fluid Mech.* **118**, 341.

MOIN, P. AND KIM, J. 1985 *J. Fluid Mech.* **155**, 441.

NARASIMHA, R. AND SREENIVASAN, K.R. 1979 *Advances in Applied Mech.* **19**, 221.

ORAN, E.S. AND BORIS, J.P. 1993 *Computers in Physics* **7**, 523.

ORSZAG, S.A. 1970 *J. Fluid Mech.* **41**, 363.

ORSZAG, S.A., PATTERSON, G.S. 1972 *Phys. Rev. Lett.* **28**, 76.

PIOMELLI, U., MOIN, P., AND FERZIGER, J.H. 1988 *Phys. Fluids* **31**, 1984.

PIOMELLI, U. FERZIGER, J.H., MOIN, P., AND KIM, J. 1989 *Phys. Fluids A* **1**, 1061.

PIOMELLI, U., ZANG, T.A., SPEZIALE, C.G., AND HUSSAINI, M.Y. 1990a *Phys. Fluids A* **2**, 257.

PIOMELLI, U., ZANG, T.A., SPEZIALE, C.G., AND LUND, T.S. 1990b In *Instability and Transition*, edited by M.Y. Hussaini and R.G. Voigt (Springer-Verlag, New York), **2**, 480.

PIOMELLI, U. AND ZANG, T.A. 1991 *Computer Phys. Comm.* **65**, 224.

PIOMELLI, U., CABOT, W.H., MOIN, P., AND LEE, S. 1991 *Phys. Fluids A* **3**, 1766.

PIOMELLI, U. 1993 In *Large Eddy Simulation of Complex Engineering and Geophysical Flows*, edited by B. Galperin and S.A. Orszag, (Cambridge University Press, Cambridge), 119.

PIOMELLI, U. 1993 *Phys. Fluids A* **5**, 1484.

PIOMELLI, U. AND LIU, J. 1995 *Phys. Fluids A* **7**, 839.

REYNOLDS, W.C. 1990 In *Whither turbulence? Turbulence at the crossroads*, edited by J.L. Lumley (Springer-Verlag, Heidelberg), 313.

ROGALLO, R.S. 1981 NASA TM 81315.

ROGALLO, R.S. AND MOIN, P. 1984 *Ann. Rev. Fluid Mech.* **16**, 99.

ROSE, H.A. 1977 *J. Fluid Mech.* **81**, 719.

SADDOUGHI, S.G. AND VERRAVALLI, S.V. 1994 *J. Fluid Mech.* **268**, 333.

SAFFMAN, P.G. 1967a *J. Fluid Mech.* **27**, 581.

SAFFMAN, P.G. 1967b *Phys. Fluids* **10**, 1349.

SCHUMANN, U. 1975 *J. Comput. Phys.* **18**, 376.

SIGGIA, E.D. AND PATTERSON, G.S. 1978 *J. Fluid Mech.* **86**, 567.

SIRIVAT, A. AND WARHAFT, Z 1983 *J. Fluid Mech.* **128**, 323.

SMAGORINSKY, J. 1963 *Monthly Weather Review* **91**, 99.

SMITH, L.M. AND YAKHOT, V. 1993 *Theoret. Comput. Fluid Dyn.* **4**, 197.

SPALART, P.R. AND WATMUFF, J.H. 1993 *J. Fluid Mech.* **249**, 337.

SPEZIALE, C.G. 1985 *J. Fluid Mech.* **156**, 55.

SQUIRES, K.D., CHASNOV, J.R. AND MANSOUR, N.N. 1994 *Proceedings of the 1994 Summer Program*, Center for Turbulence Research, 383.

STREET AND MACARAEG 1989 *Int. J. Applied Num. Math.* **6**, 123

TAFTI, D. AND VANKA, P. 1992 *Phys. Fluids A* **3**, 642.

VAN DRIEST, E.R. 1956 *J. Aerospace Sci.* **23**, 1007.

WARHAFT, Z. AND LUMLEY, J.L. 1978 *J. Fluid Mech.* **88**, 659.

WRAY, A AND ROGALLO, R.S. 1992 private communication.

YAKHOT, V. AND ORSZAG, S.A. 1986 *J. Sci. Computing* **1**, 3.

YOSHIZAWA, A. 1987 In *Encyclopedia of Fluid Mechanics*, edited by N.P. Cheremisinoff (Gulf Publishing, West Orange), **6**, 1277.

ZANG, T.A., GILBERT, N., AND KLEISER, L. 1990 In *Instability and Transition*, edited by M.Y. Hussaini and R.G. Voigt (Springer-Verlag, New York), **1**, 283.

ZANG, T.A., AND PIOMELLI, U. 1993 In *Large Eddy Simulation of Complex Engineering and Geophysical Flows*, edited by B. Galperin and S.A. Orszag, (Cambridge University Press, Cambridge), 209.